Master's thesis

NTNU
Norwegian University of Science and Technology
Faculty of Natural Sciences
Department of Materials Science and Engineering

Siri Andersen

Synthesis and Structural Stability Investigations of Mg and Nb Modified Ultra-High Ni Layered Oxides for Li-ion Batteries

Master's thesis in Chemical Engineering
Supervisor: Nils Peter Wagner
Co-supervisor: Harald Norrud Pollen
June 2022

NTNU
Norwegian University of Science and Technology

Siri Andersen

Synthesis and Structural Stability Investigations of Mg and Nb Modified Ultra-High Ni Layered Oxides for Li-ion Batteries

Master's thesis in Chemical Engineering
Supervisor: Nils Peter Wagner
Co-supervisor: Harald Norrud Pollen
June 2022

Norwegian University of Science and Technology
Faculty of Natural Sciences
Department of Materials Science and Engineering

NTNU
Kunnskap for en bedre verden

Preface

This master thesis is written as a part of the battery group in the Department of Materials Science and Engineering at the Norwegian University of Science and Technology. The project work performed during the fall semester last year has worked as a base for the further investigations in this master thesis. Large parts of the experimental work and theory is the same as for the project, but has been extended and rewritten.

I would first like to thank my supervisor Nils Peter Wagner and my co-supervisor Harald Norrud Pollen. Nils has contributed with a lot of knowledge on my research topic in general and suggested solutions to various problems arising along the way. Harald has been very helpfull in teaching me all the experimental work and provided me with synthesis methods and analysis parameters optimised for my materials. In addition I would like to thank Julian Tolchard for performing an energy-dispersive X-ray spectroscopy analysis providing me with valuable results for my thesis. I would also like to thank Matthias Schrade for making a cross section of one of my electrodes, and I would like to thank everyone responsible for the labs I have used for providing me with help when needed. Lastly, I would like to thank my friends, family and classmates for support through the semester and for much needed breaks and laughs.

Abstract

Ni-rich layered oxide cathodes have been shown to obtain a very high specific capacity leading to a large interest in them for commercial use. However, the structural instability causing a short cycle life is one of the main issues related to these materials. This thesis aimed to synthesise a Ni-rich structure to benefit from the high specific capacity, and use modification agents in an attempt to avoid rapid capacity degradation. Ni-rich layered oxide cathodes of compositions $LiNi_{0.94}Mn_{0.03}Co_{0.03}O_2$ (NMC94), $LiNi_{0.88}Mn_{0.06}Co_{0.06}Mg_{0.01}O_2$ (NMCMg88), $LiNi_{0.88}Mn_{0.06}Co_{0.06}O_2$ (NMC88) and Nb modified NMC88 (NMC88-Nb) were synthesised to investigate the annealing temperature and modification effects of Mg and Nb on the electrochemical performance. An NMC94 powder was first synthesised through an oxalic acid co-precipitation method. Annealing temperatures of 750 °C and 735 °C were utilised when heat treating the NMC94 cathodes, resulting in NMC94-750 and NMC94-735. They were then tape casted and assembled into coin cells. The 735 cathodes were assembled into half cells, and the 750 cathodes were assembled into both half cells and full cells using $Li_4Ti_5O_{12}$ (LTO) as anode material. The electrochemical results showed higher specific capacity in the 750 cells, but both cathodes had an overall poor cycling stability. The 735 cells seemed to have slightly higher capacity retention than the 750 cells, though the cycling was generally unstable providing a poor foundation for a conclusion. A comparison of an NMC94-750 full cell and an NMC88 full cell showed significantly better capacity retention for NMC88, which lead to the decision of using NMC88 as baseline material in the further investigations.

An NMCMg88 powder was synthesised by an oxalic acid co-precipitation method and two NMC88 powders synthesised by Harald Pollen were utilised in the modification investigations. The three powders were all annealed at 750 °C and ball milled on a bottle roller. One of the NMC88 powders (NMC88-1) was divided into two batches where the first batch was modified with Nb, while the second batch was post annealed without the Nb precursor to imitate the annealing from the Nb modification process (NMC88-H). Both the Mg and Nb modified cathodes and their NMC88 reference were tape casted and assembled into coin cells using graphite as anode material. Scanning electron microscopy (SEM), X-ray diffraction (XRD) and particle size distribution analysis (PSD) was performed on the cathode powders revealing a phase pure structure with similar Ni-Li mixing between the two modified structures and their reference. Energy-dispersive X-ray spectroscopy (EDS) was also performed on the NMC88-Nb cathode which revealed that the Nb had been evenly distributed in the powder likely forming $LiNbO_3$ and Nb_2O_5 on the cathode surface. Confirming a complete coating was not possible using the methods within the scope of this thesis. Electrochemical tests were done to investigate the specific capacity, coulombic efficiency and capacity retention over 95 cycles. The Mg doped cathode showed similar results to its reference though with slightly inferior performance. The Nb modified cathode showed higher capacity retention than NMC88-H, but had a lower specific capacity and higher irreversible

capacity loss. The post annealing treatment of the NMC88-H cathodes seemed to have provided the cathode with a higher specific capacity and lower capacity retention, making it useful to compare the NMC88-Nb cathode to the performance of NMC88 as well. NMC88-Nb performed inferior to NMC88 where the decreased specific capacity could be related to the formation of Nb_2O_5 or $LiNbO_3$ on the cathode surface blocking Li-diffusion pathways. An observation worth mentioning is that NMC88-Nb also underwent the post annealing process that caused decreased capacity retention in NMC88-H. Because NMC88-Nb did not suffer from as large of a decrease in capacity retention as NMC88-H, it could suggest that Nb modification of Ni-rich NMC has a stabilising effect to some degree.

All materials were compared in a cycle life extrapolation assuming constant capacity decrease, where the NMC88 reference outperformed the modified materials with a cycle life of 564. Further investigations can hopefully elaborate on the effects observed in this thesis, and contribute to obtain a more stable Ni-rich layered oxide material.

Sammendrag

Nikkel-rike lagbygde oksider har blitt bevist å kunne oppnå veldig høy kapasitet noe som har ført til stor interesse for dem i industrien. En negativ egenskap ved disse materialene er derimot den strukturelle ustabiliteten som fører til kort levetid for batteriene. Målet med denne oppgaven var å syntetisere en nikkel-rik struktur som kunne ta fordel av den høye kapasiteten samtidig som at modifisering av strukturen med Mg og Nb skulle forsøke å forhindre den raske degraderingen av kapasiteten. Nikkelrike lagbygde oksider av sammensetning $LiNi_{0.94}Mn_{0.03}Co_{0.03}O_2$, $LiNi_{0.88}Mn_{0.06}Co_{0.06}Mg_{0.01}O_2$, $LiNi_{0.88}Mn_{0.06}Co_{0.06}O_2$ og Nb modifisert NMC88 ble syntetisert og undersøkt for optimal glødingstemperatur og modifiseringseffekt av Mg og Nb på den elektrokjemiske ytelsen. Først ble et NMC94 pulver syntetisert ved bruk av en oksalsyre samutfellingsmetode. Glødingstemperaturene som ble brukt var 750 °C og 735 °C som ga opphav til navnene NMC94-750 og NMC94-735. Pulverne ble så laget til elektroder og satt sammen til knappeceller. 735 katodene ble satt sammen til halvceller og 750 katodene ble satt sammen til både halvceller og helceller ved bruk av LTO som anodemateriale. De elektrokjemiske resultatene viste høyere kapasitet hos 750 cellene, men begge katodene viste generelt dårlig syklingsstabilitet. 735 cellene syntes å ha litt høyere kapasitetbevaring enn 750 cellene, men den generelt dårlige syklingsevnen ga et dårlig grunnlag til en konklusjon. En sammenlikning av en NMC94-750 helcelle og en NMC88 helcelle viste mye bedre kapasitetbevaring for NMC88 cellen, noe som førte til beslutningen å fortsette med NMC88 som grunnlinjemateriale i de videre undersøkelsene.

Et NMCMg88 pulver ble syntetisert ved bruk av en oksalsyre samutfellingsmetode og to NMC88 pulvere syntetisert av Harald Pollen ble brukt i modifiseringsundersøkelsene. De tre pulverne ble glødet ved 750 °C og knust på en kulemølle. Et av NMC88 pulverne ble delt i to partier, hvorav det ene partiet ble modifisert med Nb og det andre ble glødet for å imitere glødingen fra Nb modifiseringsprosessen. Begge de Mg og Nb modifiserte katodenepulverne og deres referanser ble laget om til elektroder og satt sammen til knappeceller ved bruk av grafitt som anodemateriale. SEM, XRD og PSD ble utført på alle pulverne og avslørte en faseren struktur med liknende Ni-Li blanding mellom de to modifiserte strukturene og referansen deres. EDS ble også utført på NMC88-Nb pulveret noe som viste at Nb hadde jevnt over blitt fordelt i pulveret, og mest sannsynlig formet $LiNbO_3$ og Nb_2O_5 på pulveroverflaten. En bekreftelse av et fullstendig belegg på pulveret var ikke mulig å påvise gjennom metodene brukt i denne oppgaven. De elektrokjemiske testene undersøkte kapasitet, coulombisk effektivitet og kapasitetsbevaring over 95 sykler. Den Mg modifiserte katoden viste liknende resultater som referansematerialet, men med litt lavere ytelse. Den Nb modifiserte katoden viste høyere kapasitetbevaring enn referansen, men hadde lavere kapasitet og høyere irreversibelt kapasitettap i første sykel. Glødingen av NMC88-H katoden syntes å gi katoden høyere kapasitet og lavere kapasitetbevaring enn NMC88 referansen brukt i Mg modifiseringen, noe som gjør det nyttig å sammenlikne NMC88-Nb med NMC88 i tillegg. NMC88-Nb hadde generelt dårligere ytelse enn NMC88 noe som kan være relatert til former-

ing av $LiNbO_3$ og Nb_2O_5 på katodeoverflaten, noe som kan blokkere Li-diffusjonsveiene. En observasjon som er verdt å nevne er at NMC88-Nb også gjennomgikk samme gløding som NMC88-H uten å få like dårlig kapasitetsbevaring. Dette kan antyde at Nb modifiseringen kan ha en form for stabiliserende effekt på strukturen.

Alle materialene ble sammenliknet i en ekstrapolering av levetiden forutsett konstant degradering av kapasiteten, hvor NMC88 referansen utkonkurrerte de modifiserte materialene med en levetid på 564 sykler. Videre undersøkelser kan forhåpentligvis utdype de observerte effektene i denne oppgaven, og bidra til å oppnå et med stabilt nikkel-rikt lagbygd oksid.

Contents

List of Figures

List of Tables

Nomenclature

CB	Carbon Black
CCCV	Constant current constant voltage
CEI	Cathode electrolyte interphase
DEC	Diethyl carbonate
EC	Ethylene carbonate
EDS	Energy-dispersive X-ray spectroscopy
EMC	Ethyl methyl carbonate
FESEM	Field emission scanning electron microscopy
HOMO	Highest occupied molecular orbital
LCO	$LiCoO_2$
LFP	$LiFePO_4$
LIB	Lithium-ion battery
LMO	$LiMn_2O_4$
LNMO	$LiNi_{0.5}Mn_{1.5}O_4$
LNO	$LiNiO_2$
LTO	$Li_5Ti_4O_{12}$
LUMO	Lowest unoccupied molecular orbital
NCA	$LiNi_{0.8}Co_{0.15}Al_{0.05}O_2$
NMC	$LiNi_{1-x-y}Mn_xCo_yO_2$
NMC111	$LiNi_{0.33}Mn_{0.33}Co_{0.33}O_2$
NMC88	$LiNi_{0.88}Mn_{0.06}Co_{0.06}O_2$
NMC94	$LiNi_{0.94}Mn_{0.03}Co_{0.03}O_2$
NMCMg88	$LiNi_{0.88}Mn_{0.06}Co_{0.06}Mg_{0.01}O_2$
NMM94	$LiNi_{0.94}Mn_{0.03}Mg_{0.03}O_2$
NMP	1-Methyl-2-pyrrolidinone

PSD	Particle size distribution
PVDF	Polyvinylidene fluoride
SEI	Solid electrolyte interphase
SEM	Scanning electron microscopy
TM-layer	Transition metal layer
XRD	X-ray diffraction

1 Introduction

1.1 Background

The consequences of global warming have become more and more prominent the in last decade, causing droughts, floods and forest fires more frequently all across the world. The energy sector is responsible for around two thirds of the global greenhouse gas emissions which have shifted the focus onto renewable energy resources to a larger degree[1]. This has resulted in an increasing number of initiatives to replace polluting energy resources, such as fossil fuels[1]. One of those initiatives is the growing battery industry which has had a rapid development the past decade. Batteries have an advantage in that they are efficient, scalable and light in weight, which causes them to have a large variety of applications such as electric vehicles, mobile phones and computers[2]. A battery type widely used in electric vehicles today, due to its high energy density, long cycle life and good stability, is the lithium ion battery (LIB)[3], which was initially commercialised at the beginning of the 1990s[4]. The key components of LIBs that determine the performance of the batteries are the anode, the cathode and the electrolyte. The cathode is the component that governs the capacity of the battery cell[5], making it the most important component for improving the energy density of the batteries[6]. $LiCoO_2$ (LCO) is a cathode material much used in portable applications due to its mature technology, but because it suffers from structural instability and the cost of Co is high, it is not applicable in large cells[7]. In the 1990s an alternative to the LCO cathode was identified, its Ni-based isostructure $LiNiO_2$ (LNO)[7]. This structure also has a high theoretical capacity in addition to having a lower cost because Ni is cheaper than Co, making it a better alternative to LCO[7]. It does, however, also suffer from structural instability, which has made commercialisation of the LNO-based batteries difficult[7]. In an effort to stabilise the LNO-structure while simultaneously keeping the high theoretical capacity, various doping agents have been introduced to the structure partly replacing some of the Ni[7]. Two materials resulting from this research are the $LiNi_{1-x-y}Mn_xCo_yO_2$ (NMC) and $LiNi_{1-X-Y}Co_XAl_YO_2$ (NCA) cathodes, where $LiNi_{0.6}Mn_{0.2}Co_{0.2}O_2$ and $LiNi_{0.8}Co_{0.15}Al_{0.05}O_2$ are examples of cathodes shown to be viable for use in electric vehicles[7]. The automotive industry is however in need of improvement in cathode compositions to be able to have longer driving ranges and lower cost[7]. This has led to the increased research interest in cathodes with high Ni content with the optimal amount of Ni-substitution[7]. NMC and NCA cathodes with more than 80% Ni have been developed but the most optimal structure for commercialisation is yet to be found[7]. The biggest challenge is that LIBs are in general very temperature-sensitive in regards to lifetime, performance and safety[3], and when the Ni content of the cathode is increased the temperature-sensitivity also increases[8]. This is what makes the choice of doping agent and amount of doping the key focus in improving the stability of the structure.

1.2 Scope of Work

The main focus of this thesis is to look at how modification by either doping or coating of NMC cathodes with high Ni-content will affect the structural stability and performance of the batteries. In the first part of the thesis results from the specialisation project were implemented to decide on a viable baseline material. $LiNi_{0.88}Mn_{0.06}Co_{0.06}O_2$, that was previously optimised by PhD. cand. Harald Norrud Pollen, was compared to an even higher Ni containing composition of $LiNi_{0.94}Mn_{0.03}Co_{0.03}O_2$. In this thesis the effect of two different annealing temperatures, 735 °C and 750 °C, are investigated in an effort to optimise the stability of the material. In the second stage of the project NMC88 was modified by Mg doping as well as Nb surface modification based on the works of Fengxia Xin et al. [9]. The various cathode compositions were investigated physically using XRD and SEM, and electrochemically focusing on the maximal specific capacity, capacity retention and coulombic efficiency.

2 Theory

2.1 Working Principle of Li-ion Batteries

LIBs are an energy storage technology highly desired for their high energy density, decreasing cost and long lifetime, for use in e.g. electric vehicles. Li has a low reduction potential which allows the LIBs to have a very high cell potential. In addition, the Li-ion has a very small ionic radius and is one of the lightest elements in the periodic table. This allows the Li-based batteries to achieve both high power density as well as high energy density. The most important cost factors of LIBs are usually the materials of the cathode and the processing cost of the batteries[10].

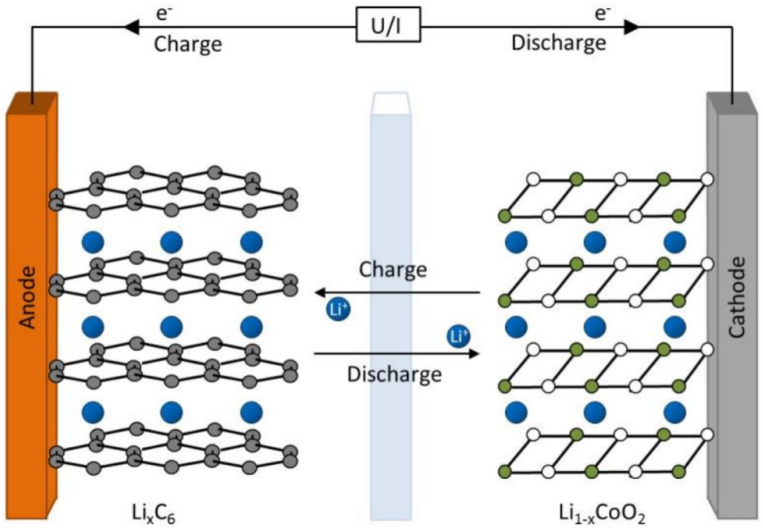

Figure 2.1: Working principle of lithium ion batteries. Aquired from [11].

Figure 2.1 illustrates the working principle of a LIB. The LIB uses Li-ions as charge carriers which are transported between two electrodes, one positive electrode referred to as the cathode and one negative electrode called anode[12]. When the Li-ions are moving from one electrode to the other, they move through an electrically insulating electrolyte[12]. The charge imbalance in the electrode causes electrons to be released and move through an external circuit[12]. The LIB is charged when the Li-ions move from the cathode to the anode, and discharged when moving from the anode to the cathode. During the discharge process is when power is generated in the LIB[12]. Using LCO as cathode and graphite as anode material, the redox reaction can be expressed as:

$$x\mathrm{Li}^+ + x\mathrm{e}^- + 6\mathrm{C} \rightleftharpoons \mathrm{Li}_x\mathrm{C}_6 \tag{1}$$

$$\mathrm{LiCoO}_2 \rightleftharpoons \mathrm{Li}_{1-x}\mathrm{CoO}_2 + x\mathrm{Li}^+ + x\mathrm{e}^- \tag{2}$$

During the charge process the reaction goes from left to right, while the discharge process goes from right to left. In total the cell reaction can be expressed as:

$$\mathrm{LiCoO_2} + 6\mathrm{C} \rightleftharpoons \mathrm{Li_{1-x}CoO_2} + \mathrm{Li}_x\mathrm{C_6} \tag{3}$$

2.2 Battery Terminology

Capacity (*Q*)

The capacity is a measurement of how long a battery can maintain a specific current before it is completely discharged. Faradays' law is used to define the theoretical specific capacity as[12]:

$$Q = \frac{1000 \cdot nF}{3600 \cdot M_w} = \frac{1000 \cdot 26.8}{M_w} \cdot n \qquad \text{[mAh/g]} \tag{4}$$

n is the number of electrons, F is the Faraday constant expressed in unit Ah/mol (96485 C/mol = 26.8 Ah/mol) and M_w being the molecular mass of the limiting electrode[12].

Electrochemical potential

The electrochemical potential can be expressed through the standard free energy (ΔG^0) as a thermodynamic measurement of the combination of both the electrostatic contribution and the energy stored as chemical potential[12]:

$$\Delta G^0 = -nFE^0 \tag{5}$$

n is the number of electrons, F is the Faraday constant and E^0 being the standard electromotive force.

Energy Density (*E*)

The definition of the energy density of a battery system is the specific energy that is stored when the battery is discharged at an appropriate current[12].

$$E = V_{oc} \cdot Q_{dis} \qquad \text{[Wh/kg]} \tag{6}$$

With V_{oc} being the open circuit voltage and Q_{dis} the discharge capacity. The energy density can be expressed as gravimetric or volumetric energy density by dividing the energy per battery by the battery weigth or battery volume, respectively. The units are typically Wh/kg for gravimetric density and Wh/L for volumetric density.

Coulombic efficiency (*CE*)

Coulombic efficiency indicates the amount of capacity loss of the battery during cycling. For each cycle it is defined as the ratio between the discharge capacity ($Q_{discharge}$) and the charge capacity (Q_{charge})[12]:

$$CE = \frac{Q_{discharge}}{Q_{charge}} \cdot 100 \qquad [\%] \tag{7}$$

C-rate

The definition of C-rate is the charge/discharge rate relative to the maximum capacity of the battery[12]. It will take $1/n$ hours to charge/discharge an entire battery if the C-rate is nC[12].

Cycle life

The cycle life of a battery is defined by the industry as the number of charges and discharges the battery can complete until the battery capacity is reduced below 80 % of the initial discharge capacity[12].

Capacity retention

The capacity retention of a battery is defined as its ability to retain the reversible capacity close to the initial discharge capacity when cycled for a large amount of cycles[12]. A high capacity retention results in a long cycle life.

Electrode loading

The electrode loading, often expressed as mg/cm^2, is defined as the amount of active electrode material[12].

2.3 Electrolytes

Different types of electrolytes typically used in Li-ion batteries are polymers, ionic liquids, liquid organic electrolytes, inorganic liquid and inorganic solid electrolytes[13]. Here the focus will be on liquid electrolytes, and the most commonly used electrolyte in LIBs is $LiPF_6$ salt dissolved in organic carbonates such as ethylene carbonate (EC), ethyl methyl carbonate (EMC) or diethyl carbonate (DEC)[13]. When selecting the proper electrolyte to use it is important to look at the stability window of the electrolyte, which is defined as the energy difference between the lowest unoccupied molecular orbital (LUMO) and the highest occupied molecular orbital (HOMO) of the given electrolyte[13]. If the electrodes have electrochemical potentials which are outside of this window, the battery will become thermodynamically unstable[13]. Figure 2.2 illustrates the energy levels of a stability window

for an electrolyte, and how the electrochemical potentials of the anode and cathode outside of this window cause reduction and oxidation of the electrolyte, respectively.

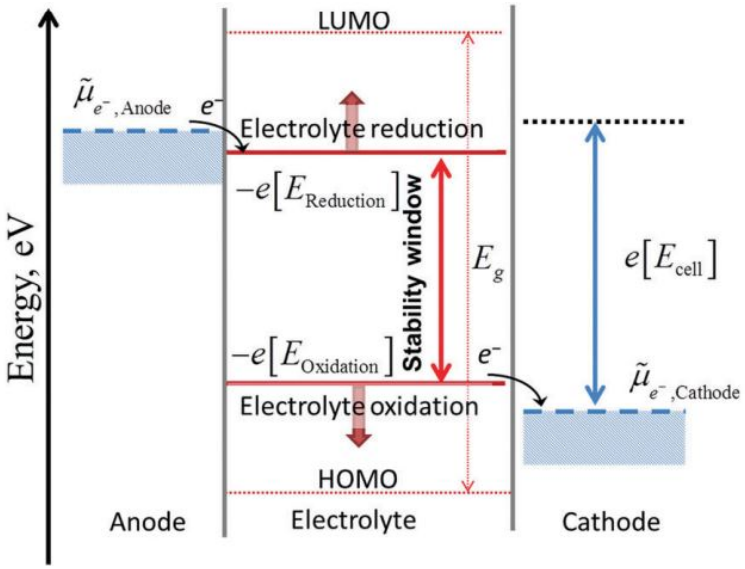

Figure 2.2: Illustration of the stability window of an electrolyte. Aquired from [14].

The formation of an electrically insulating solid electrolyte interphase (SEI) / cathode electrolyte interphase (CEI) on the boundary between the electrolyte and the anode/cathode can help kinetically stabilise the battery[13]. SEI layers are formed when the electrolyte is reduced on the anode surface, and CEI layers are formed when the electrolyte is oxidised on the surface of the cathode, which expands the electrolyte stability window as seen in Figure 2.2. Figure 2.3 illustrates how an SEI layer is formed on a graphite anode when the electrolyte $LiPF_6$ dissolved in various carbonates is reduced. The SEI layer will become thicker when cycled a few times until a stable layer has formed[15]. When the SEI layer is in place it inhibits further decomposition of the electrolyte, resulting in a longer battery life[15]. The same development applies to CEI formation on cathodes.

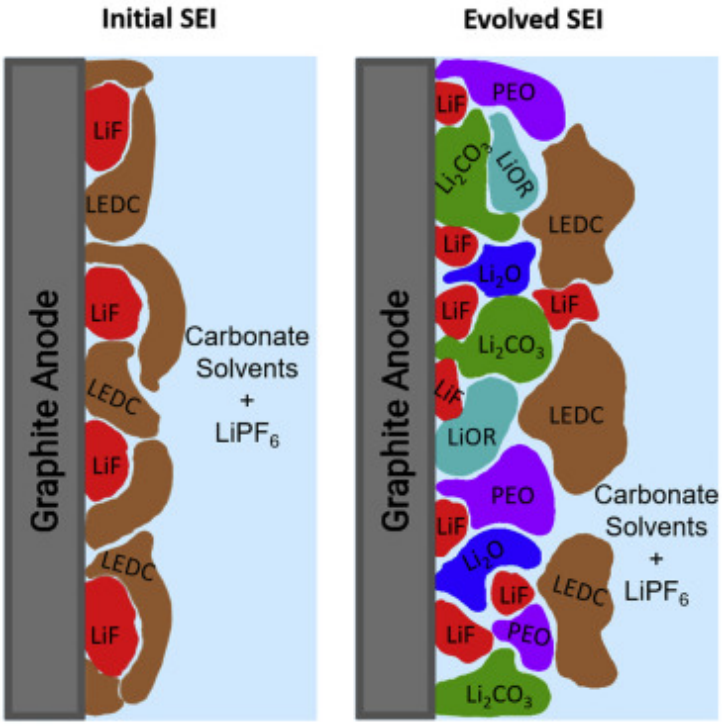

Figure 2.3: Illustration of SEI formation on a graphite anode. Aquired from [15].

2.4 Anode Materials

The properties of LIBs are also affected by the anode material in the battery, and the most common anode materials for LIBs are graphite, silicon and LTO[16]. Anode materials are normally divided into three classifications which are intercalation anodes, alloying anodes and conversion anodes[17]. Intercalation anodes such as graphite can be described by the following reaction

$$\mathrm{Li}^{+} + \mathrm{C}_6 + \mathrm{e}^{-} \rightleftharpoons \mathrm{LiC}_6 \tag{8}$$

which goes to the right during charge and to the left during discharge. Using Si as an example the reaction of alloying anodes can have the following reaction

$$15\mathrm{Li}^{+} + 4\mathrm{Si} + 15\mathrm{e}^{-} \rightleftharpoons \mathrm{Li}_{15}Si_4 \tag{9}$$

during charge and discharge. Lastly conversion anodes can be described by for example

$$\mathrm{MnO} + 2\mathrm{Li}^{+} + 2\mathrm{e}^{-} \rightleftharpoons \mathrm{Mn} + \mathrm{Li}_2\mathrm{O} \tag{10}$$

when charging and discharging a battery using MnO as anode material[17]. Graphite is a very common anode to use in LIBs due to its low working potential, however, this potential is outside the stability window of the most common electrolytes which causes SEI formation on the surface of the anode[16]. The formation of SEI causes increased cell resistance and

decreased battery capacity due to the consumption of Li[16]. These effects can be avoided by using LTO as the anode material[10]. LTO has been proven to have high rate stability and good thermal stability[10], in addition to having an intercalation potential of 1.55 V vs. Li/Li^+ which lies within the stability limit for conventional Li-ion electrolytes. For NMC based batteries it has been demonstrated that LTO anodes have much higher capacity retention compared to batteries with lithium metal or graphite as anode, for extended battery cycling [16]. However, compared to other anode materials the LTO anode has a much lower capacity which reduces the total energy density of the battery, in addition to having a high working potential and higher cost[12]. Despite these disadvantages the LTO anode has successfully been commercialised due to the advantages of its use in high power applications[10]. In comparison to LTO with a theoretical capacity of 175 mAh/g[18], graphite has a capacity of 372 mAh/g and Si has a capacity of 3580 mAh/g[19]. Though Si anodes struggle with a very large volume expansion during charging, which is why graphite is a more commonly used anode material[19].

2.5 Cathode Materials

The cathode materials play a large role in determining the total cost and energy density of LIBs[8]. Cathode materials can typically be sorted into three groups which are layered oxides, spinels and polyanionic compounds[20]. Examples of layered oxides are LCO, NMC and NCA, spinels are $LiMn_2O_4$ (LMO) and $LiNi_{0.5}Mn_{1.5}O_4$ (LNMO) and an example of a polyanionic compound is $LiFePO_4$ (LFP) which crystalises in the olivine structure[20]. These structures have different possibilities for Li-diffusion, where olivine has 1D Li-diffusion pathways, layered oxides have 2D Li-diffusion layers and spinels have 3D Li-diffusion pathways[21]. The 3D Li-diffusion pathways of spinels give these structures very high rate capabilities[21]. LFP is a commercial material with good chemical stability and electrochemical performance[21], and layered oxide cathodes are known for their high capacity[21]. The structures of each group is illustrated in Figure 2.4 where a) is the layered oxide structure of LCO, b) is a spinel LMO and c) is the polyanionic compound LFP.

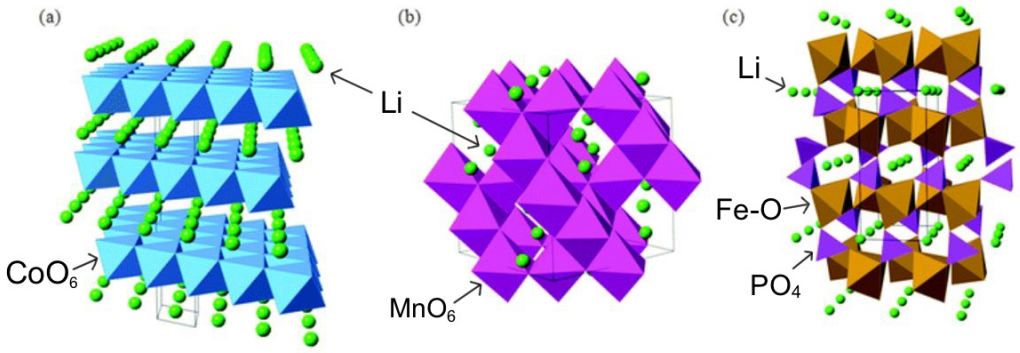

Figure 2.4: Crystal structure of various cathode materials: a) layered oxide LCO, b) spinel LMO and c) olivine LFP. Adapted from [21].

Similar to all intercalation cathodes the layered transition metal oxides function by oxidising the transition metal to a higher valence when Li is extracted from the structure, and then reducing the transition metal back to a lower valence when Li is inserted into the structure[20]. Most layered oxides will crystallise in an α-$NaFeO_2$ structure[22] with an R-3m symmetry[23]. The first layered transition metal oxide utilised as cathode material was LCO[10]. LCO has a relatively good capacity but a limitation of this material is the high Co-content, which has both high production cost and is limited in access to raw material[10]. It is also generally desirable to reduce the Co-content of batteries due to the human rights violations connected to Co-mining[24]. An alternative is to use LNO where Co is completely removed and replaced by Ni which is much cheaper[8]. However, LNO is more difficult to synthesise and has very poor thermal stability[8]. A solution introduced to solve the stability problem of the cathode has been to partly replace the Ni-content with different types of transition metals[8]. NMC and NCA are examples of cathode compositions with an experimentally good specific capacity, where Ni is partly replaced by other transition metals in the structure[10]. Both of these cathodes have Co in the structure but since the Co-content is much lower than in LCO the overall cost of the cathode material will be reduced, which is an advantage in large scale applications. $LiNi_{0.33}Mn_{0.33}Co_{0.33}O_2$ (NMC111) is an example of a cathode used in commercial batteries[10] and the potential profile of this cathode is illustrated in Figure 2.5.

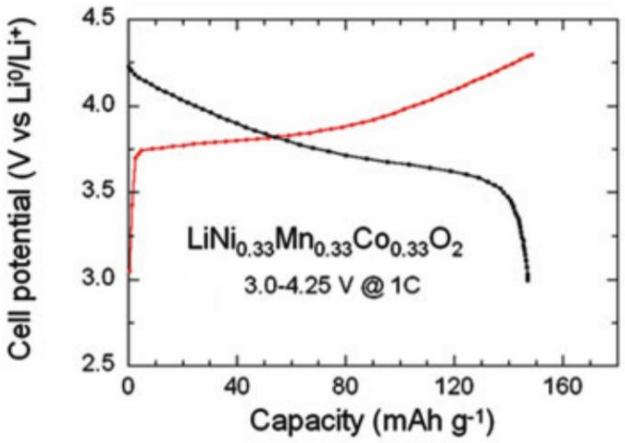

Figure 2.5: The electrochemical properties of NMC111. Aquired from [12].

2.6 Nickel Rich Layered Oxide Cathode Materials

A type of cathode that has been found to deliver high discharge capacities, making them highly desirable for use in e.g. electric vehicles, is Ni-rich layered oxide cathodes ($LiNi_{1-x}M_xO_2$)[25]. In literature Ni-rich cathodes are defined as cathodes with higher than 50 % Ni-content, while here it is defined as cathodes with Ni-content higher than 80 %. The structure of the NMC cathode material is illustrated in Figure 2.6. Here the Li-ions form layers in the structure while the transition metals Ni, Co and Mn form a transition metal layer (TM-layer) in between, with six oxygen atoms surrounding each metal-ion[26]. For Ni-rich layered oxides the TM-layer mostly consists of Ni, while the amount of different doping agents varies. This material adopts the R-3m structure which is derived from a rock-salt structure where Li-ions and metal-ions are arranged in MO_6 and LiO_6 octahedra[27]. The like cations are ordered in alternating planes along the <111> direction [27].

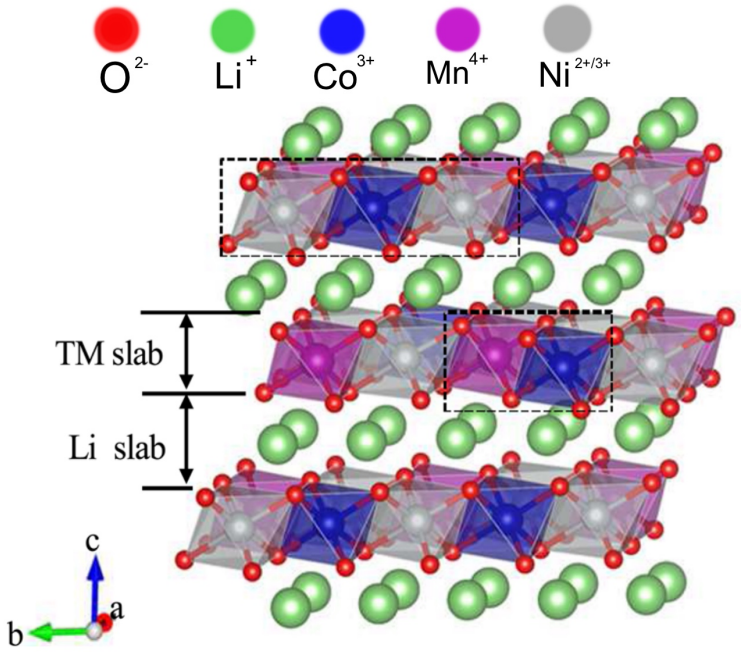

Figure 2.6: Crystal structure of an NMC cathode. Aquired from [26].

Figure 2.7 illustrates how the increased Ni-content and varying Mn- and Co-content of NMC based batteries affect the discharge capacity, capacity retention and the thermal stability of the cathode. The increasing Ni-content gives the battery a higher discharge capacity, while a higher Mn- and Co-content improve the thermal stability and capacity retention, respectively. Co has also been described as essential to achieve high rate capabilities in these materials[28].

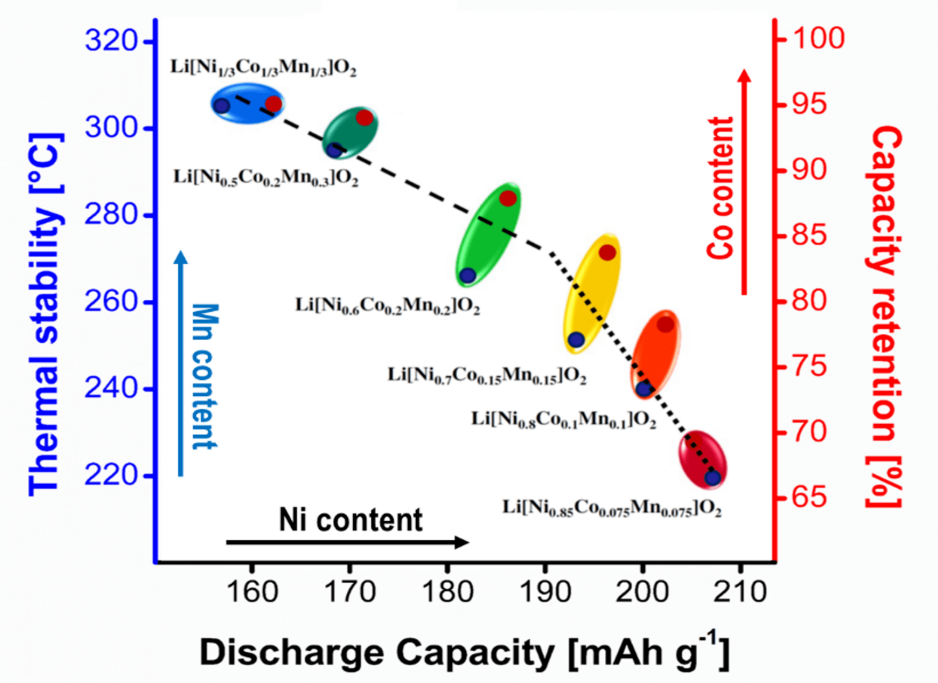

Figure 2.7: Varying Ni-, Mn- and Co-content of NMC cathodes and their effect on discharge capacity, capacity retention and thermal stability. Aquired from [8].

These types of cathodes are cheaper than LCO because the Co-content is either partly or completely replaced by Ni[29]. A downside to this cathode material is the rapid capacity fade as a concequence of the increased Ni-content. This is a negative trait for applications in e.g. electric vehicles which are dependent on the batteries to have a long cycle life[25]. The capacity fade has been proven to be caused by microcracking in the structure, due to the anisotropic volume change happening during deep delithiation[25]. This anisotropic volume change is related to the phase transitions the material undergoes which is discussed later in this section. Another challenge when it comes to the Ni-rich layered oxide cathodes is the decomposition happening when oxygen is released from the structure at higher temperatures[30]. This is a bigger challenge for these types of materials due to the high Ni-content[30]. Consequences from this decomposition could be as severe as thermal runaway, fire and explosions in the LIBs, making them a big safety hazard[29]. This happens when the increased temperature causes Ni^{3+} and Ni^{4+} to be reduced to Ni^{2+}, forming a rock salt structure and gaseous oxygen[30]. Oxygen in combination with a combustible organic liquid increases the risk of fire due to thermal runaway[30]. In addition to the safety hazards, the oxygen release happening to compensate for charge imbalance when Ni is reduced also causes oxygen vacancies to form, which in turn can lead to surface porosity and reconstructions[31]. Surface reconstruction has been observed in Ni-rich layered oxides upon charging, creating a disordered spinel structure followed by a reconstruction to a rock-salt structure[31]. This is

also considered a challenge due to its negative effects on the performance causing capacity fade, which limits the large-scale applications of the material.

Ni-rich layered oxides are very air sensitive due to their high surface reactivity when exposed to humid environments, especially in combination with CO_2-exposure[32]. The formation of Li_2CO_3 and LiOH on the cathode surface happens when the cathode is exposed to air and CO_2, and an accelerated growth rate has been observed when water is present[33]. When Li_2CO_3 decomposes at high potentials CO_2 is formed and can potentially block some of the surface of the cathode, hindering the transport of Li in this area[33]. The result of these side reactions has been shown to have degrading effects on the battery performance, causing capacity fade and increased charge transfer resistance[34]. To reduce this degradation the Ni-rich layered oxides are commonly stored and handled in a dry environment with an inert gas, such as argon or nitrogen.

Hongyang Li et al.[35] have researched the necessity of Co in Ni-rich cathodes, and found that other doping elements such as Mn, Mg and Al are good alternatives to replace Co[35]. The research was based on doping LNO with various doping elements and using Al, Mn and Mg as doping agents showed improved thermal stability in addition to Mg doping also showing improved capacity retention[35]. Looking at the cathode structure the Mn doping was observed to cause more Li-Ni interlayer mixing, where more Ni^{2+} was placed in the Li-layers of the structure to charge compensate for the higher valence Mn^{4+} in the TM-layers[35]. When doping with Al^{3+} and Mg^{2+} which are lower valence elements, the interlayer mixing of Li and Ni was reduced[35]. It is preferable to reduce interlayer mixing in the structure due to the resulting decrease in battery capacity[35]. When the Li intercalates in the TM-layer the atoms are not able to de-intercalate from the structure, causing them to become inactive upon charge and discharge[35]. However, even though Mg doping seems to prevent interlayer mixing between Li and Ni, its most preferred doping site is in the Li-layer[36]. This also has the potential to reduce the capacity of the battery depending on the amount of doping agent added to the cathode structure.

When NMC based materials with high Ni-contents are cycled the structure undergoes several phase transitions[37]. Upon charging the material transitions from a hexagonal structure to a monoclinic structure (H1-M), from monoclinic to a hexagonal structure (M-H2) and lastly from one hexagonal structure to another hexagonal structure (H2-H3)[37]. These three phase transitions are indicated in Figure 2.8 b) which is a differential capacity plot for NMC materials with 94 % Ni and 88 % Ni. Figure 2.8 a) is the voltage profile of the same materials, and the voltage plateaus in this plot correspond to the phase transition peaks in Figure 2.8 b).

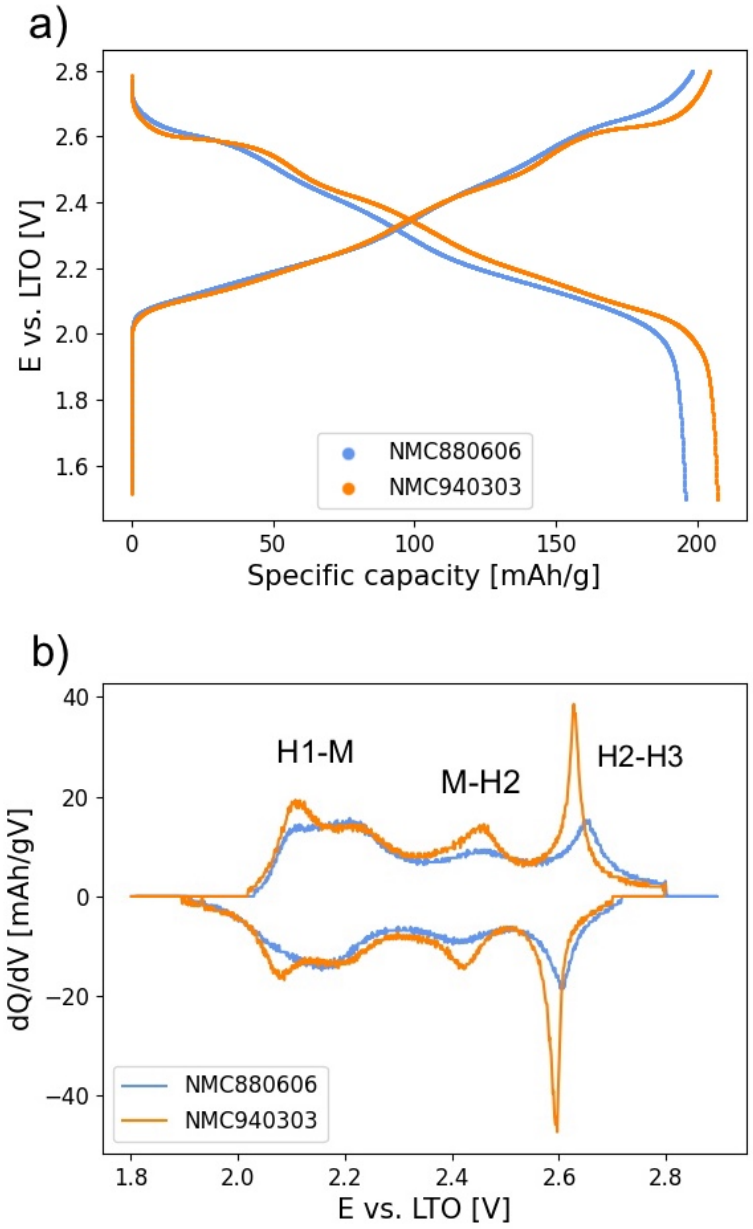

Figure 2.8: a) Voltage profile and b) differential capacity plot of NMC materials with 94 % Ni (NMC940303) and 88 % Ni (NMC880606). Aquired from [38].

Specifically the H2-H3 phase transition has been reported to affect the capacity degradation of the NMC material, due to the volume change during the transition causing microcracking in the structure[37]. When transitioning from the H2 to the H3 phase the structure rapidly collapses along the c-axis, and for NMC materials with increased Ni-content the collapse will be bigger making the material less stable[39]. As illustrated in Figure 2.8 b) the NMC material with 94 % Ni-content has a very distinct H2-H3 phase transition peak, which indicates that the material is less stable causing the discharge capacity to deteriorate

faster[40]. While for the NMC material with 88 % Ni-content the peak is more suppressed meaning that the material is more stable and the capacity will not deteriorate as quickly[37]. An NMC material with less Ni-content is much more stable but will also experience this lattice collapse when charged at high potentials[39]. The lattice collapse has been argued to be associated with the amount of Li extracted from the structure, and not the amount of Ni in the structure[39].

The introduction of Nb in Ni-rich layered oxide structures has also been investigated, and has resulted in both enhanced electrochemical performance in addition to reinforcement of the cathode structure hindering phase changes[9]. The research done by Fengxia Xin et al.[41] is based on a coating/substitution method performed post synthesis of an NMC811 material. First the NMC811 was introduced to a niobium ethoxide precursor creating a coating layer on the NMC811 particles[41]. Then a post annealing step was done at 500 °C which allowed some of the Nb-ions in the coating to diffuse into the structure of the NMC811 material[41]. Fengxia Xin et al. [9] have later proven that a post annealing temperature of 700 °C is needed to be certain that the Nb diffuses into the material. In addition to stabilizing the structure, the Nb coating/substitution of the NMC811 material showed improved initial capacity, rate capability and capacity retention, and also an overall increase in energy density of the battery due to the significant decrease in the first cycle capacity loss[41]. However, an important disadvantage to using Nb in LIBs is the high cost which limits its commercial applications.

2.7 Previous Work

A summary of results from previous, unpublished work is given below. These results are the foundation for the motivation of this thesis and will be compared with results in later sections. Three cathodes were synthesised and tested both physically and electrochemically. The three cathodes were NMC88 used as baseline, NMC94 to investigate higher Ni-content and $LiNi_{0.94}Mn_{0.03}Mg_{0.03}O_2$ (NMM94) to investigate the effect of Mg doping as replacement for Co in the structure. XRD results indicated that Mg would preferably be placed in the Li-layer of the NMM-structure, where the Li-Mg mixing was shown to be 2.9 % from the Rietveld refinements performed. The electrochemical tests shown here are performed after a 20 cycle rate test, the results are consequently based on the performance at cycle 21 - 120. The discharge capacity of the NMC88, NMC94 and NMM94 cathodes over 100 cycles at C/2 is shown in Figure 2.9, with the corresponding capacity retentions given in Table 2.1. NMC88 and NMC94 are calculated averages of two cells with standard deviation shown with error bars. The NMM94 cathode has the highest capacity retention of them all but has a lower capacity. The NMC94 cathode has the highest capacity and has a capacity retention slightly lower than NMC88 used as baseline in this project.

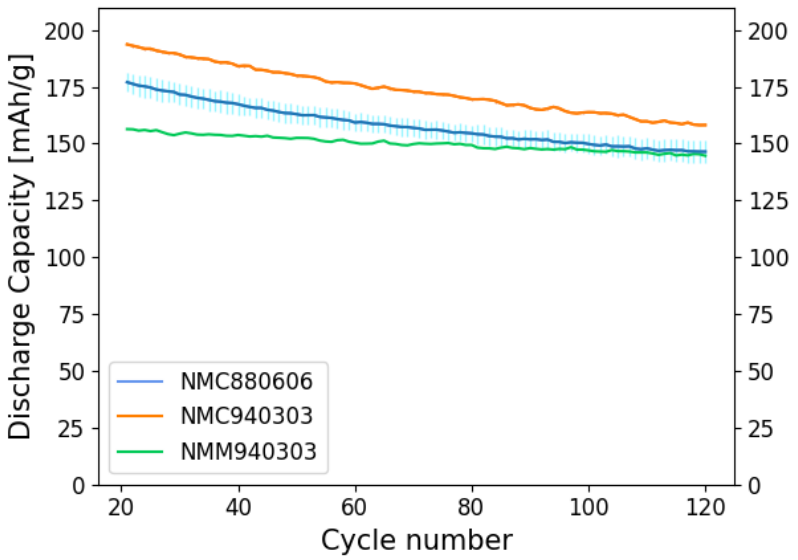

Figure 2.9: The discharge capacities of the NMC88, NMC94 and NMM94 cathodes over 100 cycles at C/2. NMC88 and NMC94 curves are given as averages of two cells with standard deviation shown with error bars.

Table 2.1: Discharge capacity retention over 100 cycles at C/2 for the three cathodes NMC88, NMC94 and NMM94.

Composition	21st cycle capacity at C/2 [mAh/g]	120th cycle capacity at C/2 [mAh/g]	Retention [%] over 100 cycles
NMC88	177	146	82.5
NMC94	194	158	81.4
NMM94	156	145	92.9

The coulombic efficiencies over 100 cycles at C/2 for the three cathodes are shown in Figure 2.10. Also here NMC88 and NMC94 are calculated averages of two cells and NMC88 has a deviating value at cycle 41 due to an abruption of the test. Average coulombic efficiencies for NMC88, NMC94 and NMM94 is 99.87 %, 99.86 % and 99.91 %, respectively.

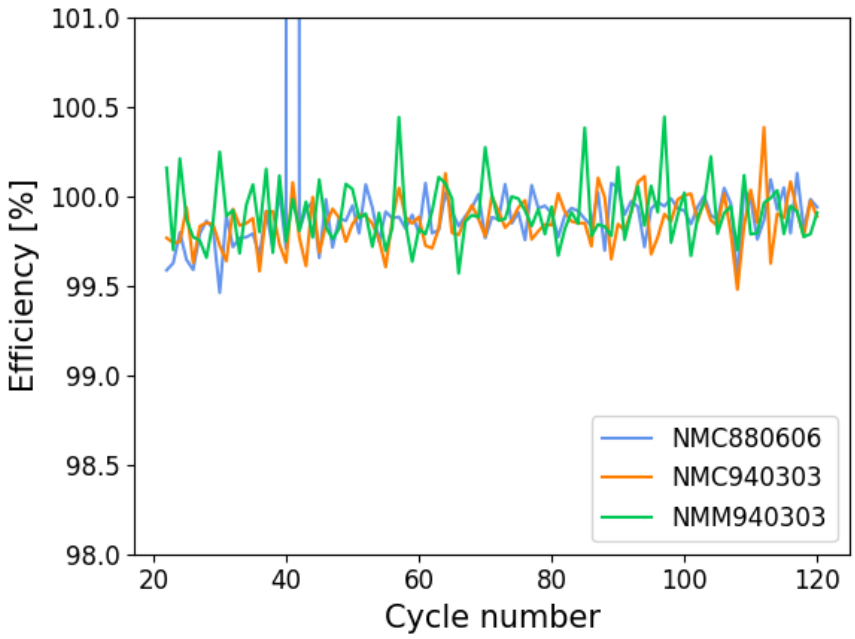

Figure 2.10: Total coulombic efficiency of NMC88, NMC94 and NMM94 for 100 cycles at C/2. The NMC88 and NMC94 curves are given as averages of two cells.

3 Experimental

In this study the effect of Mg and Nb modifications on the cyclability of Ni-rich layered oxides was elucidated. In the first phase of the study two different compositions were compared, namely $LiNi_{0.94}Mn_{0.03}Co_{0.03}O_2$ and $LiNi_{0.88}Mn_{0.06}Co_{0.06}O_2$. The NMC94 precursor was heat treated at two different temperatures, 750 °C and 735 °C, and are distinguished by using the respective names NMC94-750 and NMC94-735. A decision was made to focus on the 88 % Ni-content cathode for further investigations. In the second phase both Mg doping and Nb modification were investigated using NMC88 as baseline material. Mg doped $LiNi_{0.88}Mn_{0.06}Co_{0.06}Mg_{0.01}O_2$ was synthesised to evaluate the effects of Mg doping and will be referred to as NMCMg88. An undoped $LiNi_{0.88}Mn_{0.06}Co_{0.06}O_2$ synthesised by Harald Pollen was utilised as baseline material for NMCMg88 and is referred to as NMC88. The effect of Nb modifying was investigated by treating $LiNi_{0.88}Mn_{0.06}Co_{0.06}O_2$ (synthesised by Harald Pollen) with Nb ethoxide followed by an annealing step. The baseline compound underwent the same reannealing to elucidate the effects of this processing step. The pre treated, Nb modified and heat treated cathodes will be referred to as NMC88-1, NMC88-Nb and NMC88-H, respectively. An overview of the cathode material synthesis and post annealing steps of the different powders is illustrated in Figure 3.1 and Figure 3.2, respectively. All chemicals used in this experiment are listed in Table 3.1.

Table 3.1: Chemicals used in the experimental work.

Chemical name	Chemical Formula	Purity [%]	Supplier
Lithium nitrate	$LiNO_3$	99	Alfa Aesar
Nickel(II)acetate tetrahydrate	$Ni(CH_3COO)_2 \cdot 4H_2O$	>98	Alfa Aesar
Manganese(II)acetate tetrahydrate	$Mn(CH_3COO)_2 \cdot 4H_2O$	>99	Merck Millipore
Cobalt(II)acetate tetrahydrate	$Co(CH_3COO)_2 \cdot 4H_2O$	>98	Sigma-Aldrich
Magnesium nitrate hexahydrate	$Mg(NO_3)_2 \cdot 6H_2O$	99	Sigma-Aldrich
Oxalic acid	$C_2H_2O_4$	98	Aldrich
Ammonium hydroxide	NH_4OH	25	Emsure
Nitric acid	HNO_3	65	Sigma-Aldrich
1-Methyl-2-pyrrolidinone (NMP)	C_5H_9NO	99.5	Sigma-Aldrich
Super C65 Carbon Black (CB)	C	-	Imerys
PVDF Kynar HSV900	$(C_2H_2F_2)_x$	-	Arkema
Lithium hexafluorophosphate in EC/EMC = 50/50	$LiPF_6$ in $C_3H_4O_3$ and $C_4H_8O_3$	Battery grade	Aldrich
Lithium titanate (LTO) 2 mAh/cm^2	$Li_4Ti_5O_{12}$	Commercial battery material	Custom Cells
Niobium ethoxide	$C_{10}H_{30}NbO_5$	99.95	Sigma-Aldrich
Lithium	Li	-	-
Graphite 2.2 mAh/cm^2	C	Commercial battery material	Custom Cells

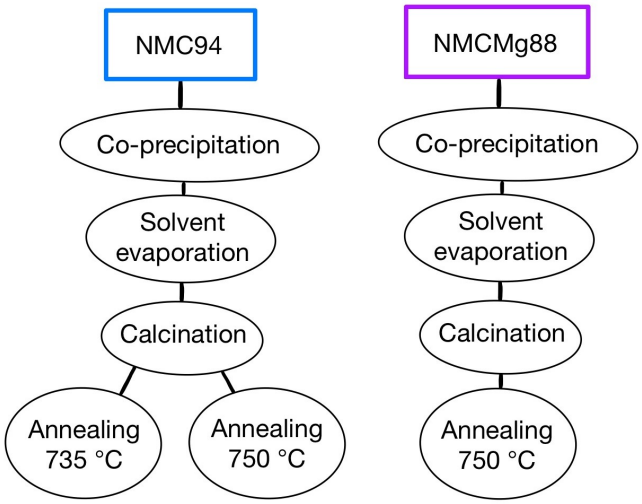

Figure 3.1: Flowchart of the cathode material synthesis of NMC94 and NMCMg88.

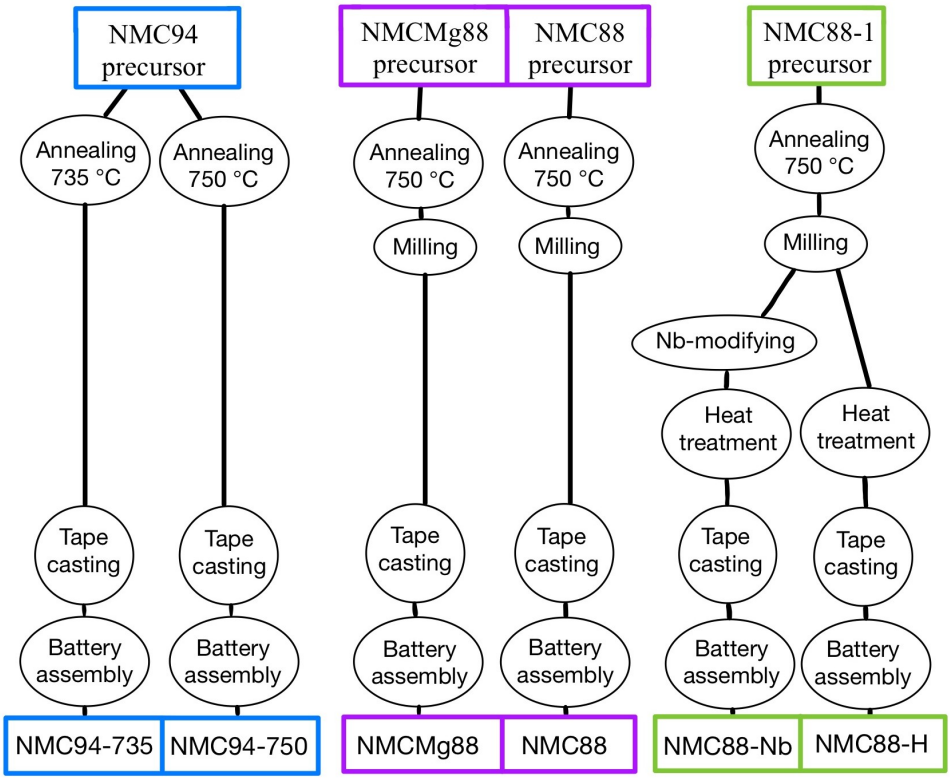

Figure 3.2: Flowchart of the post annealing steps of the cathode materials.

3.1 Cathode Material Synthesis

The cathode material synthesis was done using a single-pot co-precipitation route. The metal ion precursors corresponding to the two cathode compositions NMC94 and NMCMg88 were each added to a solution containing 250 mL DI water and 250 mL ethanol. The Li precursor was stored and weighed in an argon filled glove box and added with a 4 at% excess amount for NMC94 and a 3 at% excess amount for NMCMg88. Precursors of Ni, Mn, Co and Mg were used as received and added in stoichiometric amounts. Previous work by Harald Pollen et al.[42] showed good stoichiometry control by using acetate precursors. The mixed metal ion solutions were heated to 60 °C on a hot plate and the pH was adjusted to 3 using HNO_3 and NH_4OH.

Two other solutions containing 250 mL DI water and 250 mL ethanol were added oxalic acid powder in excess amounts. These solutions were also heated to 60 °C on a hot plate, and using NH_4OH and HNO_3 the pH was adjusted to 3. The amounts of all the precursors added are listed in Table 3.2.

A dropping funnel was utilised to drip the metal ion solution into the oxalic acid solution for each composition, using a drop rate of $\sim$ 0.1 mL/s (2 drops/s) at 60 °C and under

Table 3.2: The amount and molar amount of the various precursors added in the synthesis of NMC94 and NMCMg88.

Precursors	NMC94		NMCMg88	
$LiNO_3$	3.5855 g	0.052 mol	3.5505 g	0.0515 mol
$Ni(CH_3COO)_2 \cdot 4H_2O$	11.6964 g	0.047 mol	10.9490 g	0.044 mol
$Mn(CH_3COO)_2 \cdot 4H_2O$	0.3676 g	0.0015 mol	0.7354 g	0.003 mol
$Co(CH_3COO)_2 \cdot 4H_2O$	0.3739 g	0.0015 mol	0.7474 g	0.003 mol
$Mg(NO_3)_2 \cdot 6H_2O$	-	-	0.1280 g	0.0005 mol
$C_2H_2O_4$	18.6810 g	0.2075 mol	18.6813 g	0.2075 mol

continuous stirring at 300 rpm. Both the drop rate and the pH was controlled and re-adjusted every 30 minutes.

When the solutions were completely mixed they were set on a hot plate for 18 hours with continuous stirring at 300 rpm and a temperature of 60 °C. After this the hot plate was adjusted to 150 °C, keeping the stirring rate at 300 rpm until the solvents were fully evaporated. The precipitates were then mortared to a fine powder and stored in a desiccator.

A calcination furnace (Nabertherm L-052K2RN) was used to calcine the precipitates at 450 °C for 5 hours, using a heating and cooling rate of 200 °C/h. The calcined precursors were then mortared and stored in a desiccator until further heat treatment. The next heat treatment was an annealing done in an Entech double tube furnace with oxygen flow (6NL/h). For the NMC94 powder two different temperatures were used, 735 °C and 750 °C, resulting in the powders NMC94-735 and NMC94-750, respectively. These powders were heat treated for 15 hours, with a heating rate of 200 °C/h and a cooling rate of 300 °C/h shown in Figure 3.3 a).

The NMCMg88, NMC88-1 and NMC88 powders were all heat treated at 750 °C for 25 hours, with both heating and cooling rate of 200 °C/h. The heat treatment of these powders is illustrated in Figure 3.3 b). The finished heat treated powders were transferred to a glove box with argon atmosphere where they were mortared once more before they were stored inside the glove box until further use.

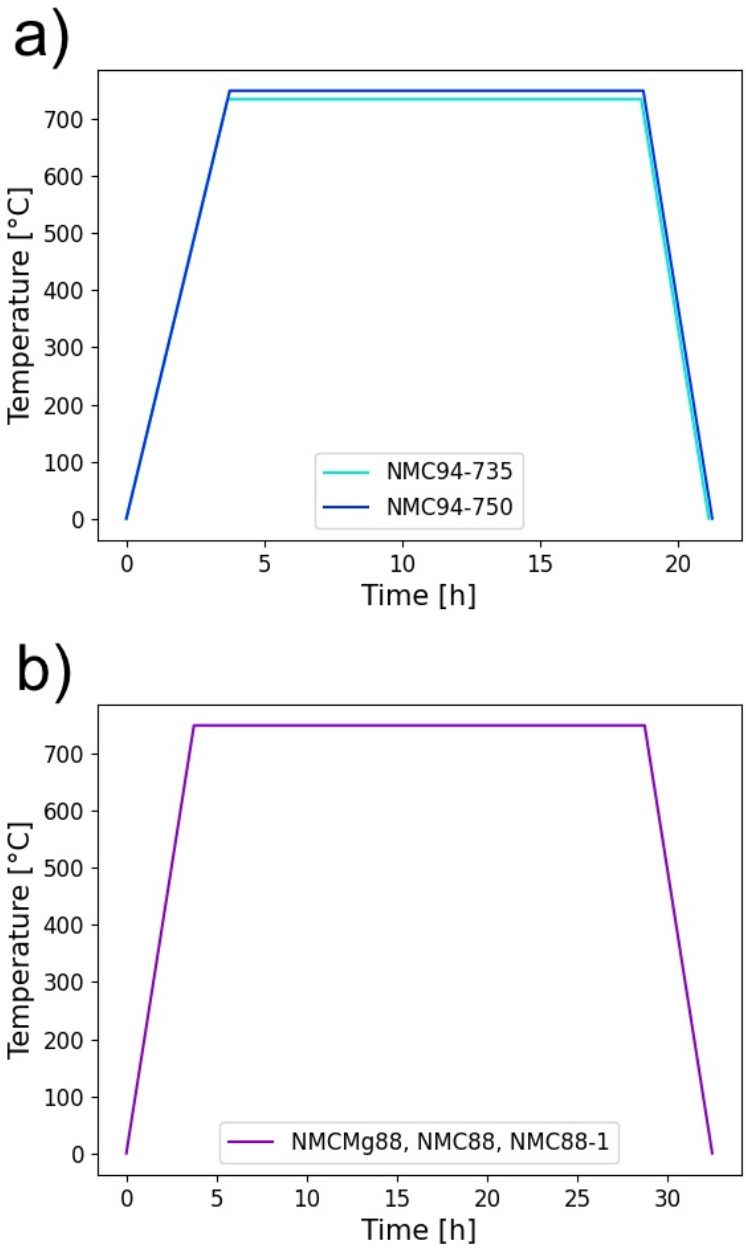

Figure 3.3: Temperature vs time for annealing of a) the two NMC94 powders and b) the NMCMg88, NMC88 and NMC88-1 powders.

The particle size distribution of the three powders NMCMg88, NMC88-1 and NMC88 were analysed through laser diffraction using a Horiba Partica LA-960 with isopropanol as the dispersant. Afterwards the powders were deagglomerated by ball milling on a roller bench using zirconium oxide balls (= 5 mm) in isopropanol inside a plastic container. The milling was done on a Tecnotest bottle roller at 100 rpm for 1 hour and the powder was then dried using a hot plate. Laser diffraction was performed to verify the deagglomeration.

3.2 Nb Modification

The Nb modification was based on a study by Fengxia Xin et al.[41] where the authors found that a 500 °C annealing step mainly resulted in a surface coating with limited diffusion into the bulk of the material. The assumption was made that the Nb would react with surface Li species forming $LiNbO_3$. The goal was to aim for approximately 2 wt% $LiNbO_3$. To calculate the amount of Nb ethoxide required the molecular weight of $LiNbO_3$ (147.846 g/mol) and the molecular weight and density of $Nb(OCH_2CH_3)_5$ (323.25 g/mol / 1.268 g/mL) were used.

NMC88-Nb was synthesised by dispersing 2 g NMC88-1 into 100 mL ethanol containing 87.5 mg Nb ethoxide. The solution was then set to stir on a hot plate for 18 hours with a stirring rate of 200 rpm and no heating to allow for hydrolysis of the Nb ethoxide. Afterwards the temperature was set to 150 °C evaporating the solvents and leaving the Nb treated powder. The Nb treated and an untreated control sample (NMC88-1) were both heat treated in the same tube furnace used earlier, resulting in NMC88-Nb and NMC88-H, respectively. The heat treatment was done at 500 °C for 3 hours with oxygen flow (6NL/h), with both the heating and the cooling rate at 200 °C/h as illustrated in Figure 3.4.

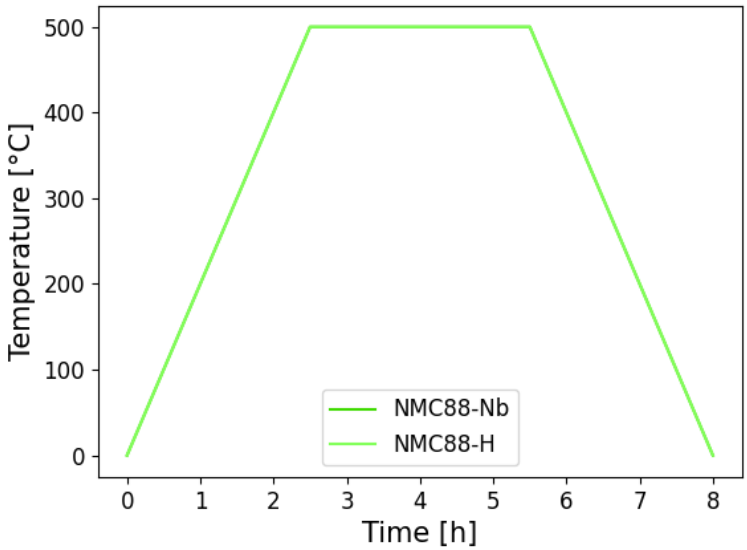

Figure 3.4: Temperature vs time for heat treatment of NMC88-Nb and NMC88-H.

3.3 X-Ray Diffraction Analysis

To analyse the phase composition and structure of all materials, an X-ray diffraction analysis was done using a D8 Advance A 25 DaVinci with a LynxEye XE detector, a CuKα radiation source, a divergence slit of 0.2 ° and Bragg-Brentano geometry. The sample preparation was done on a Si-flat sample holder with vacuum grease. The Rietveld refinements based

on earlier works by Harald Pollen et al.[42] were performed in Topas (version 5) with the structures fitted to an α-$NeFeO_2$ structure with an R-3m space group, refining both the lattice parameters and site occupancies. The samples were assumed stoichiometric, with the initial positions of the different compounds assumed as listed in Table 3.3, only calculating the oxygen position. For all samples the cation disorder was assumed in which Li and Ni were able to switch positions, Mn and Co would only exist in the TM-layer and Mg was able to switch position from the Li-layer to the TM-layer in the NMCMg88 sample.

Table 3.3: The assumed structural position of the compounds used as initial values for the Rietveld analysis.

Compound	x	y	z	Layer	Site
Li	0.000	0.000	0.000	Li-layer	3a
Ni	0.000	0.000	0.500	TM-layer	3b
Mn	0.000	0.000	0.500	TM-layer	3b
Co	0.000	0.000	0.500	TM-layer	3b
Mg	0.000	0.000	0.000	Li-layer	3a
O	0.000	0.000	0.245	-	6c

3.4 Scanning Electron Microscopy Analysis

The morphology of all samples was analysed by field emission scanning electron microscopy (FESEM) using a Zeiss Supra 55VP. This was done after the synthesis of the NMC94-735 and NMC94-750 powders, in addition to both before and after milling of the NMCMg88, NMC88-1 and NMC88 powders. The NMC88-Nb and NMC88-H powders were also analysed after the modifying and heat treatment, respectively. The sample preparation was done by attaching the powders to a sticky carbon base before inserting the sample holder into the vacuum chamber. The micrographs were taken at magnification 100X, 1000X, 10kX and 20kX, with 10.0 kV operating voltage and current 118 µA.

The NMC88-Nb sample was also analysed by energy-dispersive X-ray spectroscopy where the amount of Nb was investigated in the powder sample. The EDS was done with an operating voltage of 10.0 kV and with a current of 133.0 µA. An additional SEM EDS was performed by Julian Tolchard on a Hitachi S-3400N using a secondary electron detector with operating voltages of 7.0 kV and 20.0 kV.

3.5 Electrode Fabrication

Electrodes of all samples were made through tape casting. Slurries consisting of 90 wt% active material, 5 wt% carbon black (CB) and 5 wt% polyvinylidene fluoride (PVDF) were mixed using 1-Methyl-2-pyrrolidinone (NMP) as solvent. The PVDF was added through a pre-made binder solution which consisted of 5 wt% PVDF and 95 wt% NMP. The mixing

of the slurries was done in zirconium oxide containers with three zirconium oxide balls, which were shaken in a Retsch MM400 shaker mill. For NMC94-735 and NMC94-750 the CB and binder solutions were first mixed at 25 Hz for 15 minutes, before the active material and additional NMP were added and shaken at 25 Hz for 40 minutes. The slurries were then tape casted onto aluminium foil using a 200 µm gap applicator on a K Control Coater K101. For the Mg doped and Nb modified sample and their reference samples all components of the slurry were added in the same step and mixed for 45 minutes at 25 Hz. The slurries were then tape casted using a 220 µm gap applicator. The tape casts were all dried overnight in a vacuum drying furnace at 120 °C and then stored inside a glove box with an argon atmosphere. Table 3.4 shows the amounts of components added to all six cathode compositions, and the resulting wt% of active material is shown in Table 3.5.

Table 3.4: Amounts of the compounds used in tape casting of all cathodes.

Set	Compound	Active material [g]	CB [g]	Binder solution [g]	NMP [g]
94 % Ni	NMC94-735	1.0003	0.0558	1.1310	0.9
	NMC94-750	1.0000	0.0556	1.1189	0.9
Mg doping	NMCMg88	1.5001	0.0830	1.6740	0.2
	NMC88	1.5000	0.0833	1.6858	0.2
Nb modifying	NMC88-Nb	1.5004	0.0836	1.6763	0.2
	NMC88-H	1.5001	0.0835	1.6828	0.2

Table 3.5: The wt% of active material for all cathodes.

Set	Compound	Active material [wt%]
94 % Ni	NMC94-735	89.90
	NMC94-750	89.96
Mg doping	NMCMg88	89.99
	NMC88	89.95
Nb modifying	NMC88-Nb	89.96
	NMC88-H	89.95

3.6 Coin Cell Assembly

The six different cathodes were assembled into 2016 coin cells with coin cell tops, bottoms, gaskets and spacers from Hohson. For NMC94-735 and NMC94-750 both half cells and full cells with LTO anodes (2 mAh/cm^2, Custom Cells) were made. The half cells were assembled using 0.3 mm spacers and full cells were assembled using 1 mm spacers. The NMCMg88, NMC88, NMC88-Nb and NMC88-H cathodes were all assembled in full cells using graphite

(2.2 mAh/cm^2, Custom Cells) as anode material and 1 mm spacers. The graphite anodes were cut into 18 mm diameter disks and the N/P ratio of the cells was approximately 1.1. The N/P ratio is based on 2.2 mAh/cm^2 graphite and 230 mAh/g NMC, and assuming 16 mm diameter electrodes. All cathodes were cut into 16 mm diameter disks and the separators used were Celgard 2325 separators with 19 mm diameter. The electrolyte used was 60 µL 1 M $LiPF_6$ in EC/EMC 50/50 by volume, and the finished assembled coin cells were crimped in a crimper for 4 s.

3.7 Battery Cell Testing

Electrochemical tests were performed on the finished coin cells to investigate their specific capacity, coulombic efficiency and capacity retention. For the NMC94-735 and NMC94-735 cathodes the tests were done on a Biologic BCS-805 battery cycler at a temperature of 25 °C. The test program used was a 100 cycle test at charge and discharge rate C/2 with the three first cycles at C-rate C/10. For the half cells the cut-off voltages were set to 3.0 - 4.3 V and for the LTO full cells the cut-off voltages were set to 1.5 - 2.8 V. At the end of the charge the coin cells were kept at 4.3 V or 2.8 V, for half cells and full cells respectively, until the current dropped to C/10 (CCCV). 1 C is defined as 180 mA/g.

The Mg doped and Nb modified cathodes and their reference were tested on a Lahne CT2001A LAND Battery Testing System at 25 °C. These cells were tested for 95 cycles at C/3 and the first two initial formation cycles were performed at a slow rate of C/20 to allow for SEI formation on the graphite anode. The 95 cycles were done in sets of 25 where the cells were cycled at C-rate C/10 for two cycles before every set and also at the end of the test. The cut-off voltages were set to 2.9 - 4.2 V, and at the end of every charge the cells were kept at 4.2 V until the current dropped to C/10 (CCCV). 1 C was also here defined as 180 mA/g. The loading of all the different cathodes is shown in Table 3.6.

One coin cell of each cathode was made separately to investigate the specific capacity, coulombic efficiency and irreversible capacity loss of the first cycle at C/20.

Table 3.6: The amount of active material and loading of all cathodes, given a 16 mm diameter disk. The loading is an average of a given number of cathodes.

Set	Compound	Active material [mg]	Loading [mg/cm^2]	# cells
94 % Ni	NMC94-735	4.825 ± 1.348	2.40 ± 0.67	2
	NMC94-750	9.852 ± 2.020	4.90 ± 1.00	7
Mg doping	NMCMg88	17.05 ± 2.225	8.48 ± 1.11	4
	NMC88	18.30 ± 0.300	9.10 ± 0.15	4
Nb modifying	NMC88-Nb	18.78 ± 1.200	9.34 ± 0.60	3
	NMC88-H	18.53 ± 0.780	9.22 ± 0.39	4

4 Results

4.1 Temperature Investigations of NMC94

4.1.1 Scanning Electron Microscopy of NMC94

The primary particles of the two NMC94 powders were investigated and Figure 4.1 shows SEM micrographs of them taken at a magnification of 20 kX. For both powders the primary particles vary in size, but the majority have a diameter of less than 1 µm. The primary particles have also agglomerated into bigger secondary particles.

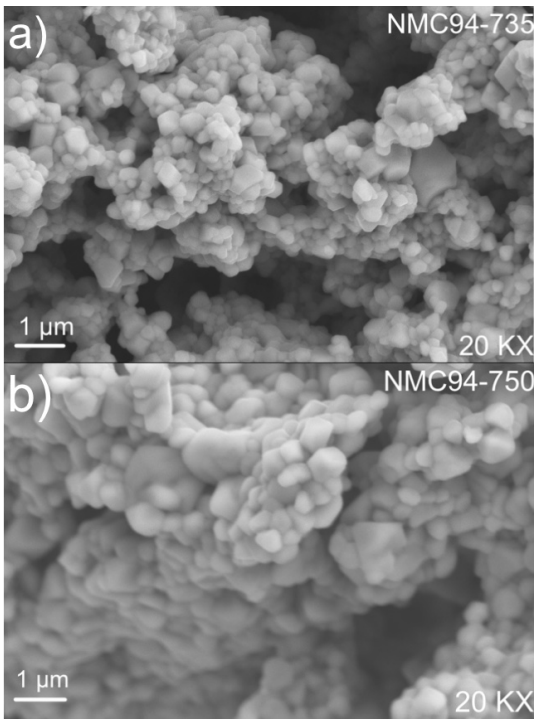

Figure 4.1: SEM micrographs of a) NMC94-735 and b) NMC94-750 taken at magnification 20 kX.

4.1.2 X-Ray Diffraction of NMC94

X-ray diffractograms of the NMC94 powders heat treated at 735 °C and 750 °C are shown in Figure 4.2. In both cases, no extra reflections were observed. The calculated crystallographic data obtained by Rietveld refinements to the R-3m space group are shown in Table 4.1. The oxygen position and the a- and c-values are approximately the same for both powders. Calculated values for the Ni-Li side disorder were 3 % for NMC94-735 and 1.7 % for NMC94-750. These numbers might have significant error but show a clear trend.

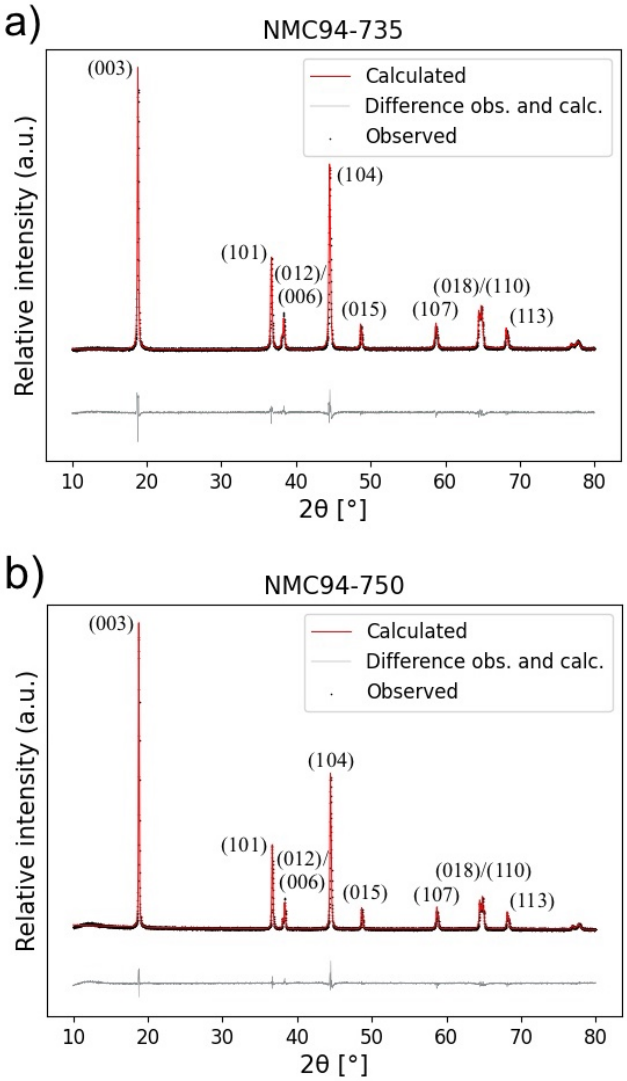

Figure 4.2: X-ray diffractograms of a) NMC94-735 and b) NMC94-750.

Table 4.1: Calculated crystallographic data obtained by Rietveld refinements of NMC94-735 and NMC94-750.

Composition	a [Å]	c [Å]	O (z-coordinate)	Ni_{Li} [%]	Rwp
NMC94-735	2.88	14.19	0.242	3.0	5.1
NMC94-750	2.88	14.20	0.241	1.7	5.3

4.1.3 Battery Cell Testing of NMC94

The first and second cycles of NMC94-735 and NMC94-750 half cells are illustrated in Figure 4.3. The specific capacity of the 750 cell is higher than for the 735 cell, though the

capacity of the first cycle in the 750 cell is slightly lower than the second cycle. The voltage plateaus at 4.2 V corresponding to the H2-H3 phase transition is visible in both cathodes.

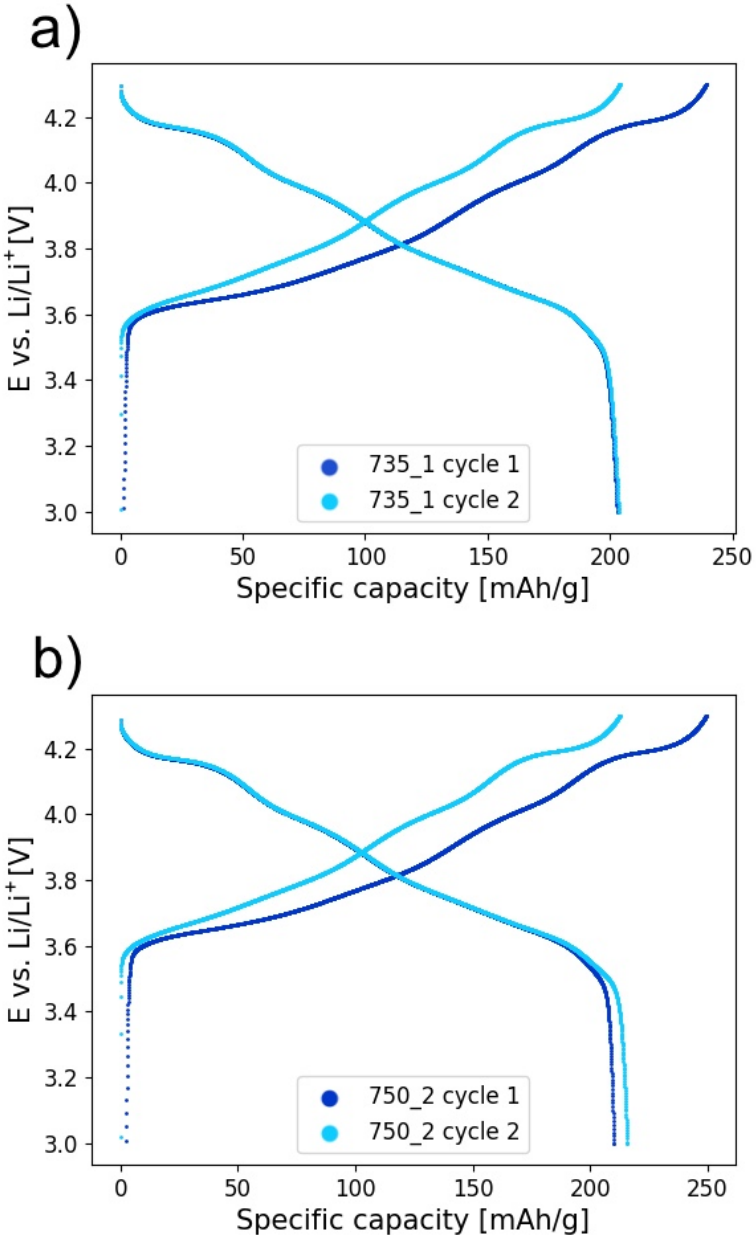

Figure 4.3: Voltage profile of the first and second cycle for half cells of a) NMC94-735 and b) NMC94-750, cycled at C/10 with cut-off voltages set to 3.0 - 4.3 V.

Figure 4.4 shows the discharge capacity over 100 cycles for the different coin cells containing NMC94-735 and NMC94-750 cathodes, a) being half cells of both cathodes and b) being full cells of NMC94-750 using LTO as anode material. The half cells had cut-off voltages of 3.0 - 4.3 V and the LTO full cells had cut-off voltages of 1.5 - 2.8 V. The full cells were made in an in an effort to improve the poor stability observed in the half cells. All cells

were cycled at a temperature of 25 °C. The charge and discharge rate for the cycling program was C/2, with the three first cycles charging and discharging at C/10. During cycling all the coin cells, except for the half cells 735-1, 750-1 and 750-2, were interrupted causing a drop in discharge capacity and disturbance in the curves. The 735-2 half cell also experiences additional disturbance around cycle number 50 - 70, which is most likely caused by a bad connection with the coin cell holder. The cycling program for all three full cells and the 735-2 half cell were stopped around cycle 94, while the 750-3 and 750-4 half cells were stopped around cycle 90. The capacity retention for each cell is summed up in Table 4.2 where the 750 full cells had the best retention around 65-66 %, the 750 half cells had poor retention at 37-43 % and the 735 half cells were in between at 50-54 % capacity retention.

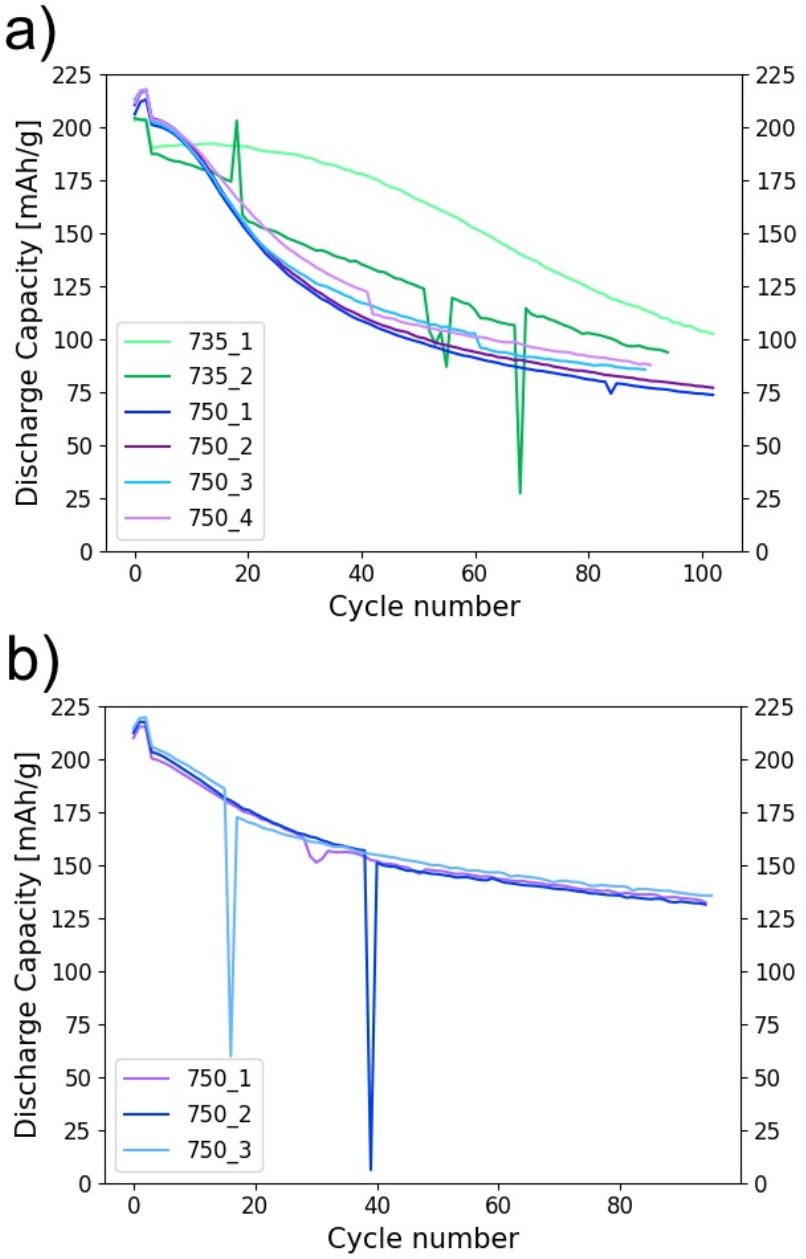

Figure 4.4: The discharge capacity of the different coin cells with NMC94-735 and NMC94-750 cathodes, cycled for 100 cycles at C/2 with the three first cycles cycled at C/10. a) shows half cells and b) shows full cells using LTO as anode material.

The coulombic efficiency of the NMC94-735 and NMC94-750 half cells is shown in Figure 4.5. The 750 cell has generally lower coulombic efficiency throughout the cycling program, cycling at around 98 % while the 735 cell mainly cycled at above 99 %.

Table 4.2: The discharge capacity and capacity retention of the different NMC94-735 and NMC94-750 coin cells.

Coin cell	1st cycle capacity at C/10 [mAh/g]	1st cycle capacity at C/2 [mAh/g]	last cycle capacity at C/2 [mAh/g]	Retention [%] over 90-100 cycles
735-1	203	190	102	53.8
735-2	204	187	94	50.0
750-1	206	201	74	36.6
750-2	210	204	77	37.7
750-3	213	202	85	42.2
750-4	211	203	88	43.0
750-LTO-1	210	200	132	66.1
750-LTO-2	212	203	131	64.6
750-LTO-3	214	206	135	65.8

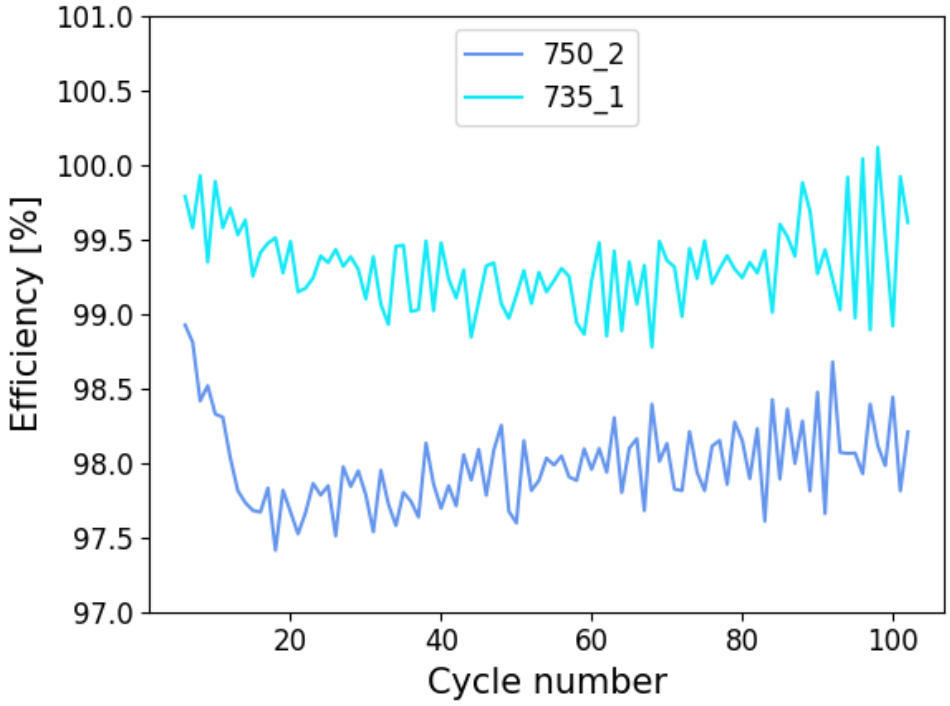

Figure 4.5: The coulombic efficiency of NMC94-735 and NMC94-750 half cells cycled at C/2 for 100 cycles.

4.2 Modification Investigations

4.2.1 Particle Size Analysis

A PSD analysis was done on the NMC88-1, NMCMg88 and NMC88 powders before and after milling, and the resulting data is shown in Figure 4.6. All three powders had bimodal distribution pre milling with a large peak at around 10-20 µm and a small peak between 60-100 µm. Previous SEM investigations of NMC94 suggest that both peaks correspond to agglomerates. The aim of milling the powders was to crush the big secondary agglomerates and generate an agglomerated powder with monomodal size distribution. Post milling all three powders had only a distribution peak for the small agglomerates which was at around 5-6 µm. The differences in agglomerate size before and after milling of the NMC88-1 powder are visualised in the overview SEM micrographs in Figure 4.7. All three powders showed the same agglomerate size differences in the SEM analysis, which can be seen in Figure A.2 and Figure A.3 in the Appendix.

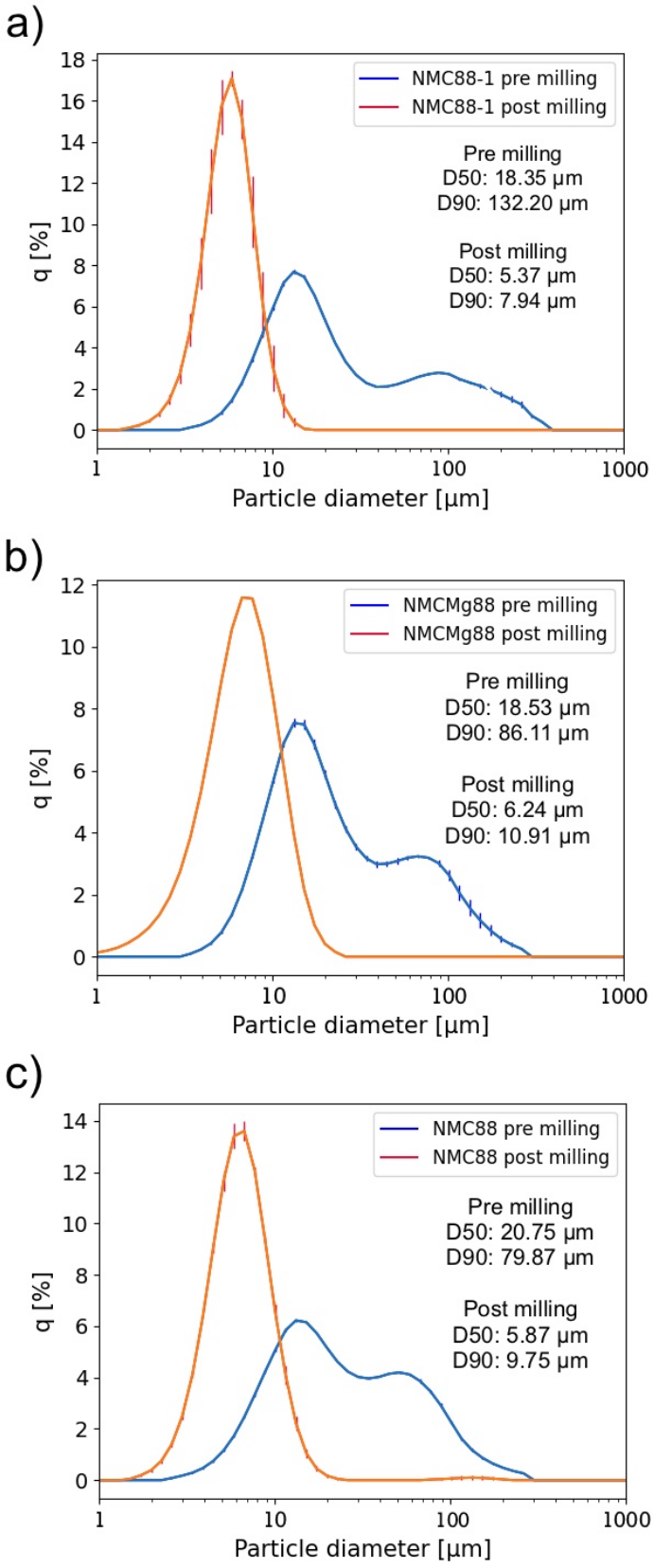

Figure 4.6: Particle size distribution before and after milling of a) NMC88-1, b) NMCMg88 and c) NMC88, including D50 and D90 values.

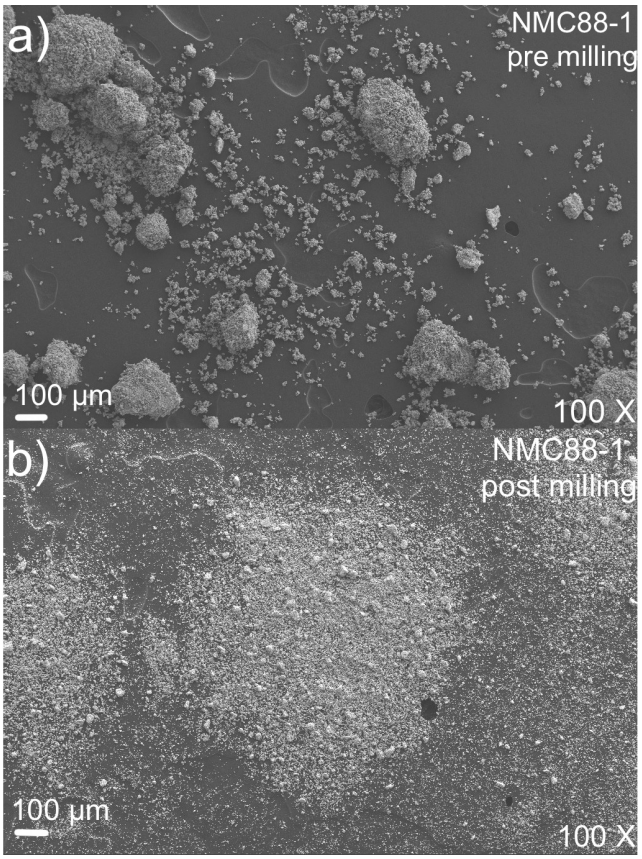

Figure 4.7: SEM micrographs showing the NMC88-1 powder a) before and b) after milling, taken at magnification 100X.

The final cathode powders of NMCMg88, NMC88, NMC88-Nb and NMC88-H were also analysed using SEM, and the micrographs taken at magnification 20 kX are shown in Figure 4.8. All four powders had primary particles of varying sizes but all had a diameter of less than 1 µm.

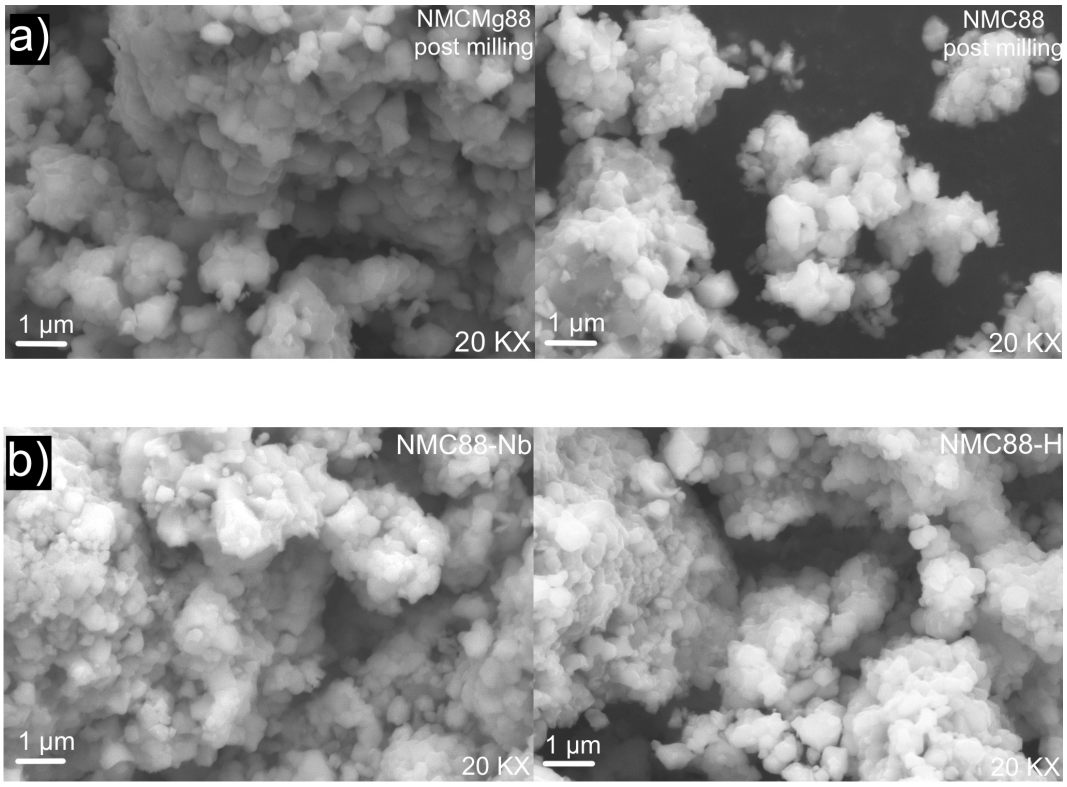

Figure 4.8: SEM micrographs of a) NMCMg88 and NMC88 and b) NMC88-Nb and NMC88-H taken at magnification 20 kX.

4.2.2 X-Ray Diffraction of NMC88 Powders

Refined X-ray diffractograms taken of the four NMC88 cathode powders are shown in Figure 4.9 and Figure 4.10. All reflections could be indexed to the layered α-$NaFeO_2$ structure with R-3m space group. The corresponding calculated crystallographic data which were obtained by Rietveld refinements are shown in Table 4.3. The a- and c-values are approximately the same for all powders, and the oxygen position does not vary significantly. However, the amount of cation site disorder varies slightly between the different cathode compositions. For NMC88-1, the Ni-Li site disorder starts at 3 % but shows a slightly decreasing trend with the modifying and heat treatment, as can be seen in the results for NMC88-Nb and NMC88-H. For NMCMg88 and its reference material, the Ni-Li site disorder is the same at 2.2 %. Mg was assumed to be placed in the Li-layer because this gave a better fit in the previous project work[38], and also due to its size. The Rietveld refinements showed that 0.7 % of the Mg was placed in the Li-layer of the NMCMg88 structure.

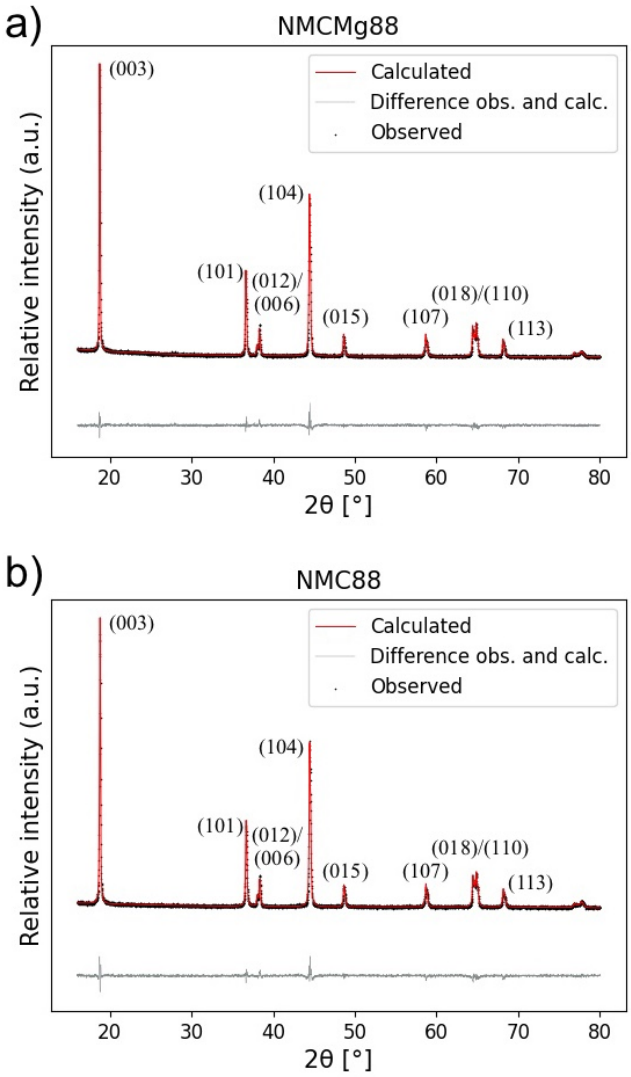

Figure 4.9: X-ray diffractograms of a) NMCMg88 and b) NMC88.

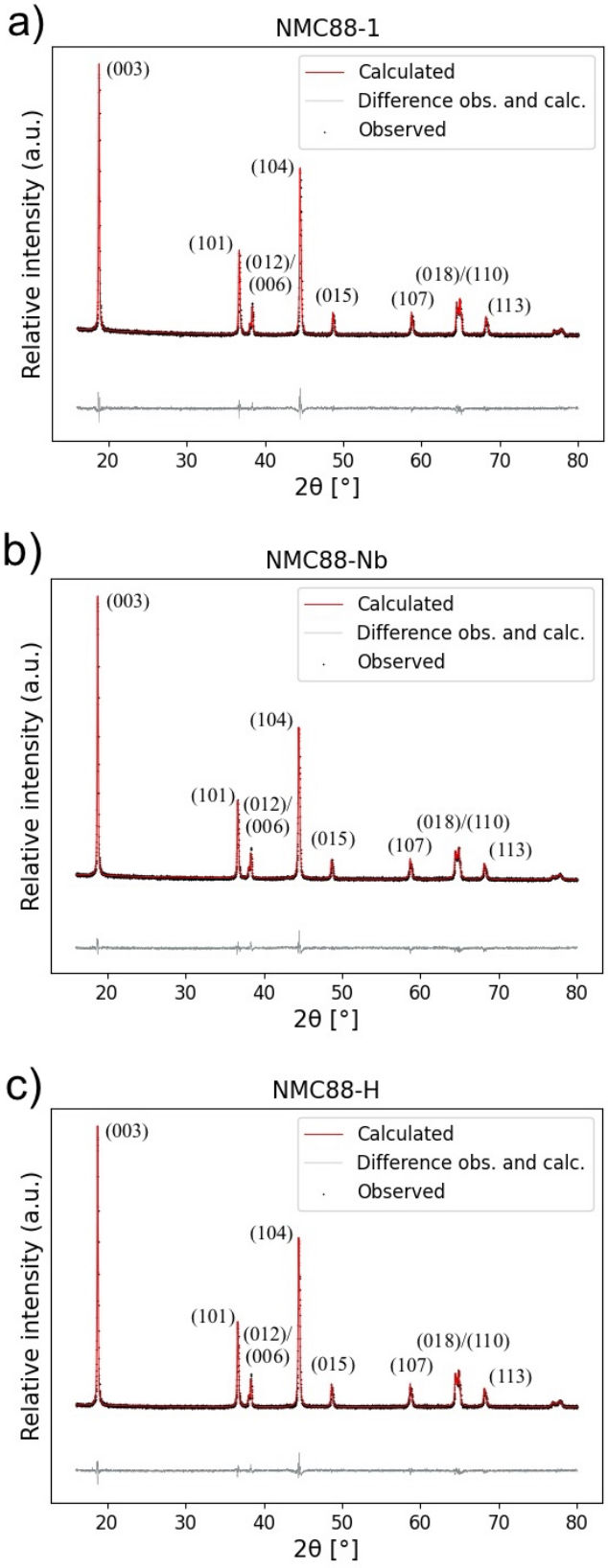

Figure 4.10: X-ray diffractograms of a) NMC88-1, b) NMC88-Nb and c) NMC88-H.

Table 4.3: Calculated crystallographic data obtained by Rietveld refinements of the Mg doped powder and its reference, and the NMC88-1, Nb modified and heat treated powder.

Set	Composition	a [Å]	c [Å]	O (z-coordinate)	Ni_{Li} [%]	Mg_{Li} [%]	Rwp
Mg doping	NMCMg88	2.87	14.20	0.241	2.2	0.7	5.168
	NMC88	2.87	14.20	0.241	2.2	-	4.989
Nb modifying	NMC88-1	2.87	14.20	0.242	3.0	-	5.165
	NMC88-Nb	2.88	14.20	0.241	2.8	-	4.806
	NMC88-H	2.87	14.20	0.242	2.9	-	4.535

4.2.3 Energy-Dispersive X-Ray Spectroscopy of NMC88-Nb

Energy-dispersive X-ray spectroscopy was performed to analyse if the Nb had been evenly dispersed in the cathode powder. The three zones investigated in the first EDS analysis of the NMC88-Nb sample are shown in Figure 4.11. One area and two spots were investigated and the compounds detected are listed with amounts and error in Table 4.4. EDS spectra of the different zones can be found in Appendix B. The quantification of the compounds in Table 4.4 is only indicative of the real values as the EDS analysis is not optimal for powder samples.

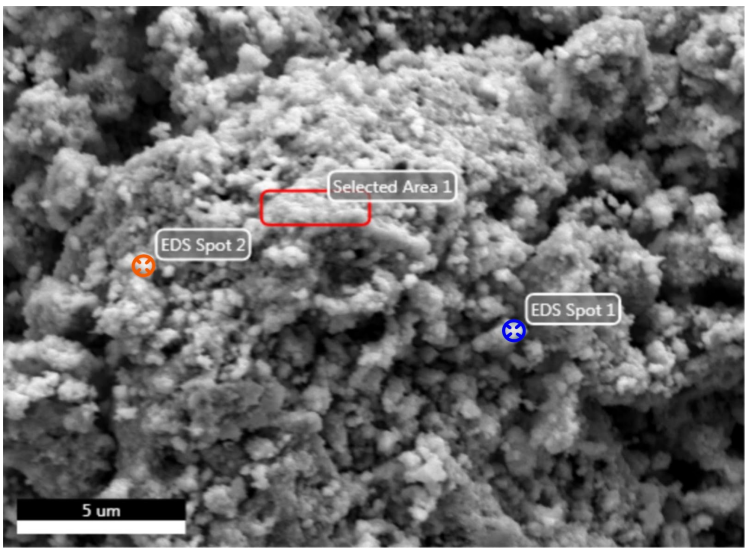

Figure 4.11: SEM micrograph of the EDS analysis zones in the NMC88-Nb powder. Area 1 is indicated in red, spot 1 is indicated in blue and spot 2 is indicated in orange.

Table 4.4: EDS analysis results from the powder sample of NMC88-Nb showing the amounts of the different compounds detected.

Detection zone	Compound	at%	Error [%]	Amount [%]
Area 1	Nb	0	-	0
	Ni	18.91	3.87	87.22
	Mn	1.44	9.68	6.64
	Co	1.33	13.32	6.13
Spot 1	Nb	3.18	2.99	24.54
	Ni	8.56	4.64	66.05
	Mn	0.66	18.40	5.09
	Co	0.56	16.71	4.32
Spot 2	Nb	2.02	5.71	9.18
	Ni	17.33	4.13	78.74
	Mn	1.39	10.71	6.32
	Co	1.27	16.10	5.77

EDS mappings performed by Julian Tolchard are shown in Figure 4.12 and Figure 4.13. The first mapping in Figure 4.12 was an overview mapping performed with an operating voltage 20.0 kV, where a) is a SEM micrograph of the mapped area and b) is the Nb mapping. The overview mapping shows one hotspot of Nb, but otherwise shows an evenly distributed Nb signal in the powder.

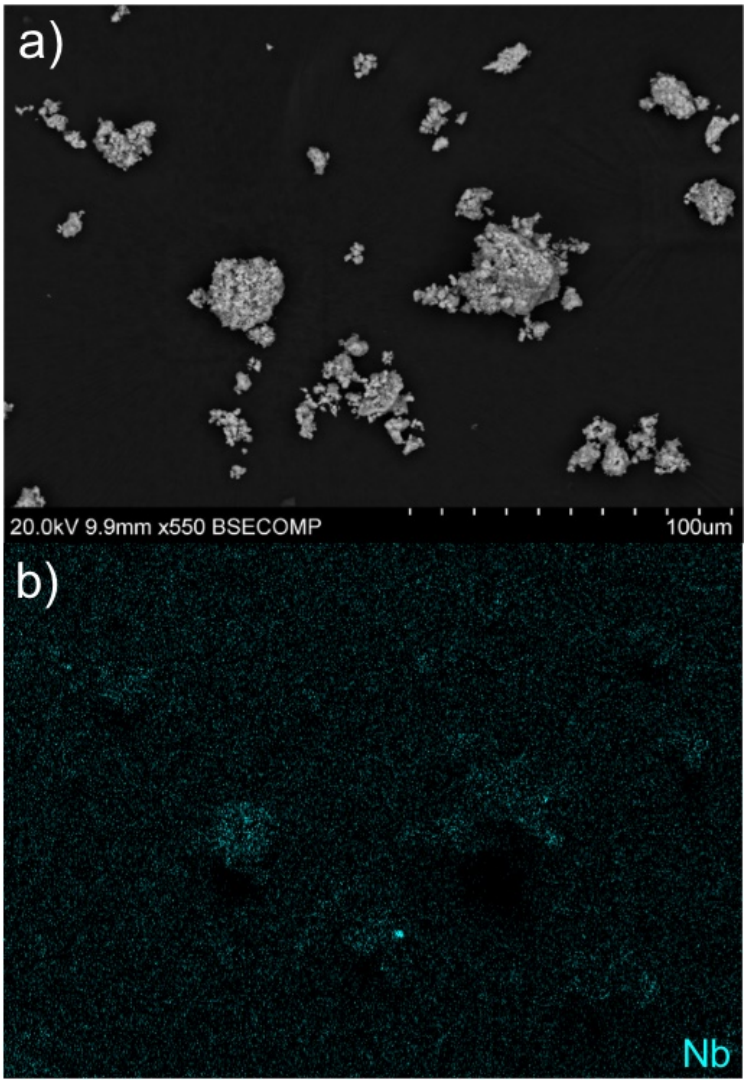

Figure 4.12: EDS mapping performed by Julian Tolchard at operating voltage 20.0 kV. a) is a SEM micrograph of the mapped area and b) is the Nb mapping.

The second mapping in Figure 4.13 is a close-up of one of the secondary particles in the overview mapping, performed with an operating voltage of 7.0 kV. The SEM micrograph of the mapped area is shown in a) and b) shows the Nb mapping. The mapping indicates that Nb is present all over the secondary particle though an even coating is not possible to confirm using this analysis method.

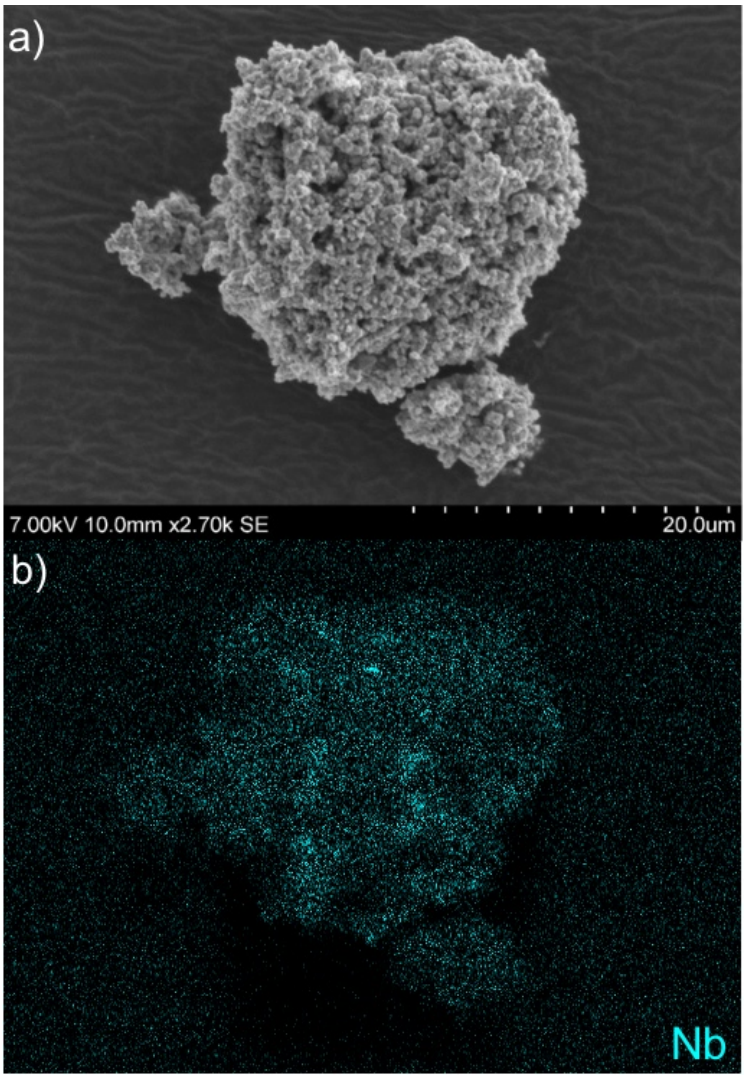

Figure 4.13: EDS mapping performed by Julian Tolchard with an operating voltage of 7.0 kV. a) is a SEM micrograph of the mapped area and b) is the Nb mapping.

An EDS point analysis also performed by Julian Tolchard on the secondary particle in Figure 4.13 is shown in Figure 4.14. The indicative amounts of the different compounds detected in spectrum 40, 41 and 43 are listed in Table 4.5. EDS spectra of spectra 40, 41 and 43 can be found in the Appendix B.

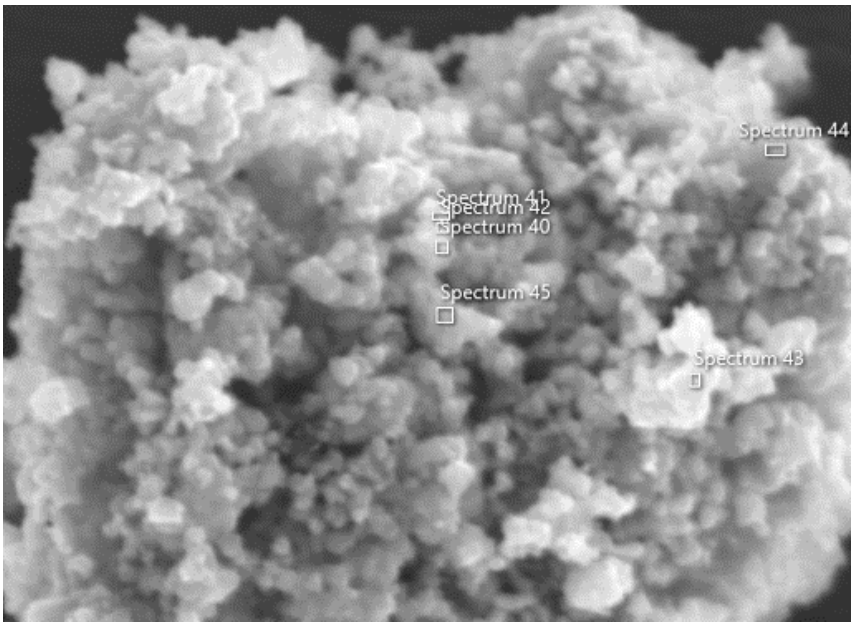

Figure 4.14: SEM micrograph of the EDS analysis zones in the NMC88-Nb powder performed by Julian Tolchard.

Table 4.5: EDS analysis results from the powder sample of NMC88-Nb performed by Julian Tolchard.

Detection zone	Compound	at%
Spectrum 40	Nb	1.6
	Ni	57.74
	Mn	3.55
	Co	4.2
Spectrum 41	Nb	4.76
	Ni	49.27
	Mn	3.21
	Co	3.49
Spectrum 43	Nb	0.41
	Ni	56.91
	Mn	3.59
	Co	4.11

4.2.4 Battery Cell Testing of NMC88 in Graphite Full Cells

All four NMC88 cathode powders were made into thick electrodes which can be challenging. Figure 4.15 shows a SEM micrograph of a cross section of an NMC88-Nb electrode. The

thickness of this electrode is measured to be around 60 µm, though it varies due to the roughness of the electrode surface.

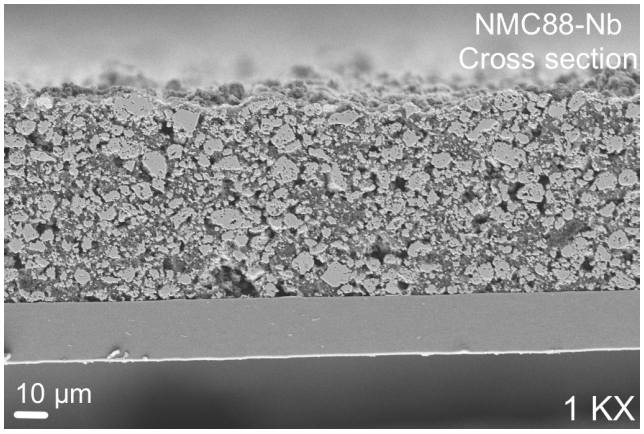

Figure 4.15: SEM micrograph of a cross section of an NMC88-Nb electrode taken at magnification 1 kX.

Mg Doping Investigation

The voltage profile of the first and second cycle of the NMCMg88 and NMC88 graphite full cells cycled at C/20 is shown in Figure 4.16 a) and b), respectively. The specific capacity, coulombic efficiency and the irreversible loss of the first cycle is given in Table 4.6. In both cathodes the voltage plateaus corresponding to the H2-H3 phase transition are visible around 4.1 V.

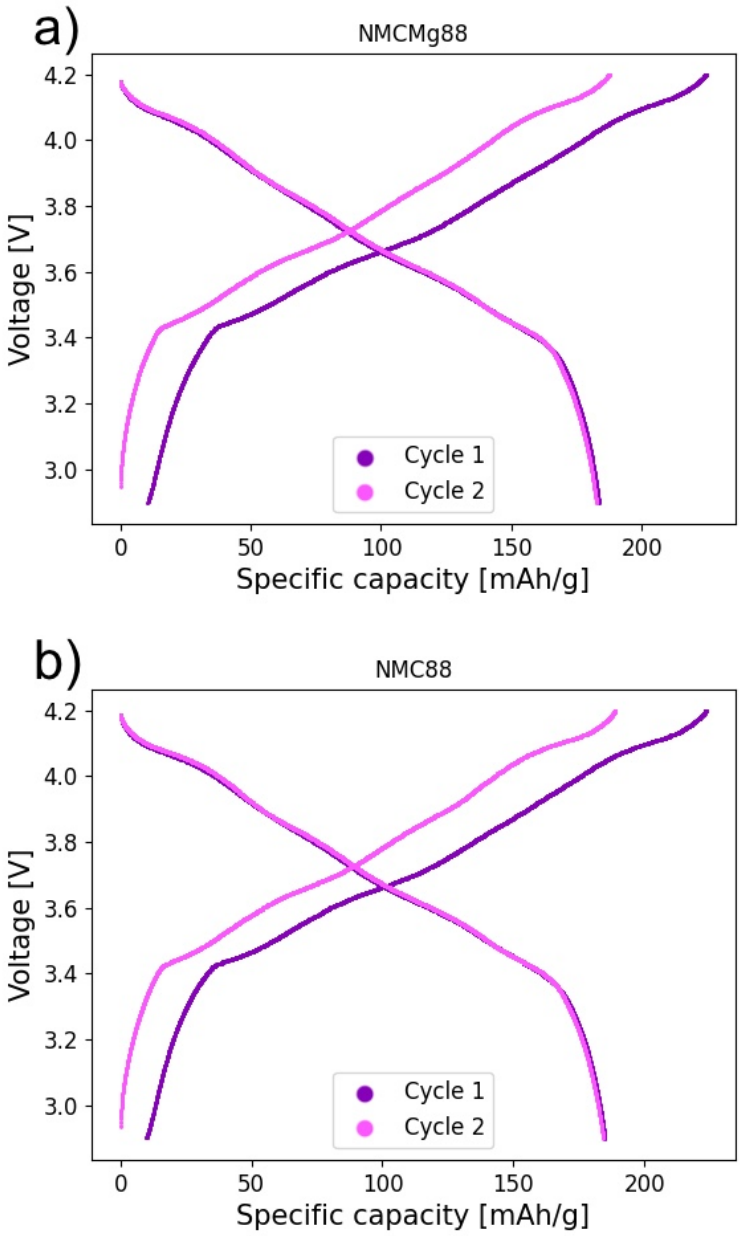

Figure 4.16: Voltage profile of the first and second cycle of a) NMCMg88 and b) NMC88 graphite full cells. Both cathodes were cycled at C/20 and the cut-off voltages were set to 2.9 - 4.2 V.

Figure 4.17 shows the cycling stability after the formation of NMCMg88 and NMC88 cycled at C/3 for 95 cycles, illustrated as an average of a number of coin cells with standard deviations shown through error bars. Due to an error in the battery cycler, the formation cycles for most cells stopped at a lower cut-off voltage than programmed and switched to C/10 at varying cycles. The cells were restarted with an updated program after a cycler restart at cycle 40. The capacity retention for the two cathodes is given in Table 4.7.

Table 4.6: The first cycle capacity, coulombic efficiency and capacity loss for the Mg doped cathode and its reference, cycled at C/20.

Composition	Specific capacity [mAh/g]	Coulombic efficiency [%]	Irreversible capacity loss [mAh/g]
NMCMg88	184	82	33.7
NMC88	185	83	32.0

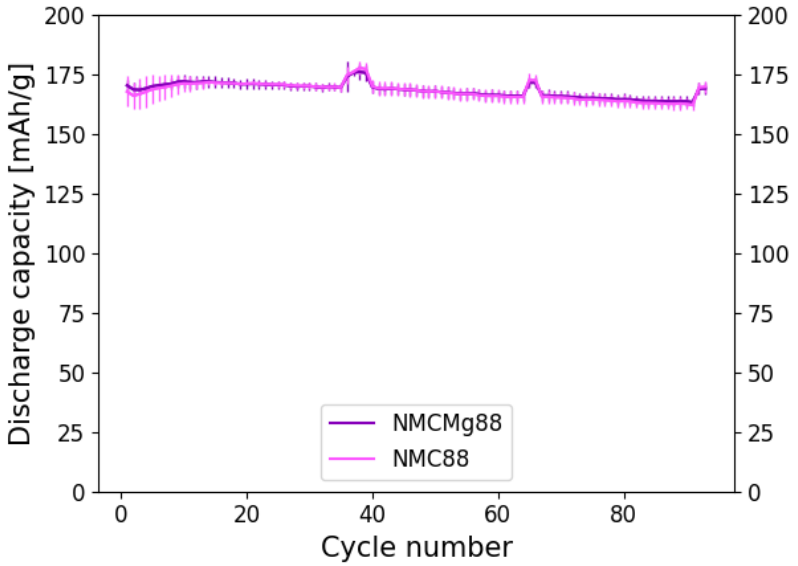

Figure 4.17: Discharge capacity for NMCMg88 and NMC88, cycled at C/3 for 95 cycles. The C-rate was C/10 for two cycles for every 25th cycle, starting at cycle 38. The discharge capacity is given as an average of several coin cells with standard deviation shown with error bars.

Table 4.7: The discharge capacity retention of NMCMg88 and NMC88.

Composition	1st cycle capacity at C/3 [mAh/g]	last cycle capacity at C/3 [mAh/g]	Retention [%] over 95 cycles
NMCMg88	170	163	95.9
NMC88	168	162	96.7

The discharge capacities for cycle 41, 68 and 95 cycled at C/10 for NMCMg88 and NMC88 is shown in Figure 4.18. Both cathodes show similar capacity retention at this C-rate.

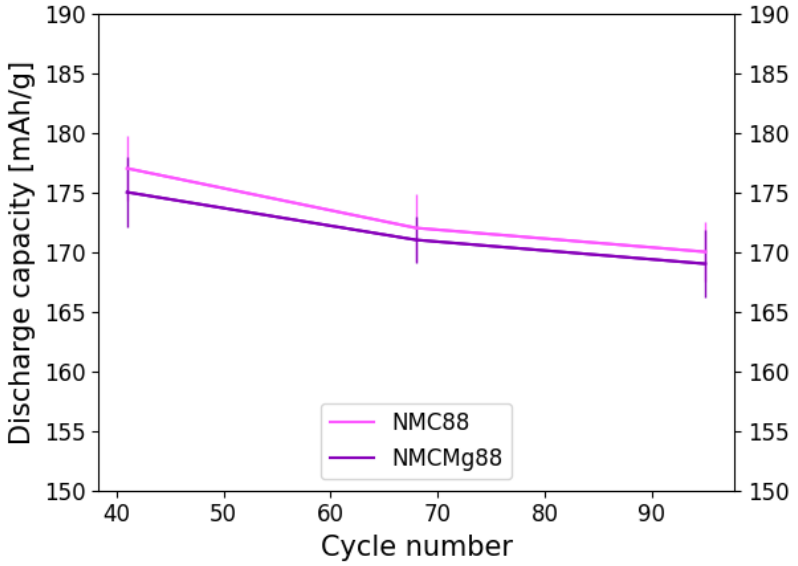

Figure 4.18: Discharge capacities for NMCMg88 and NMC88 at cycle 41, 68 and 95, cycled at C/10.

Figure 4.19 shows the coulombic efficiency of NMCMg88 and NMC88 cycled at C/3 for 95 cycles. The two cathodes show similar efficiency performance throughout, with the expected increase and decrease in the cycle ranges where the C-rate was adjusted to C/10.

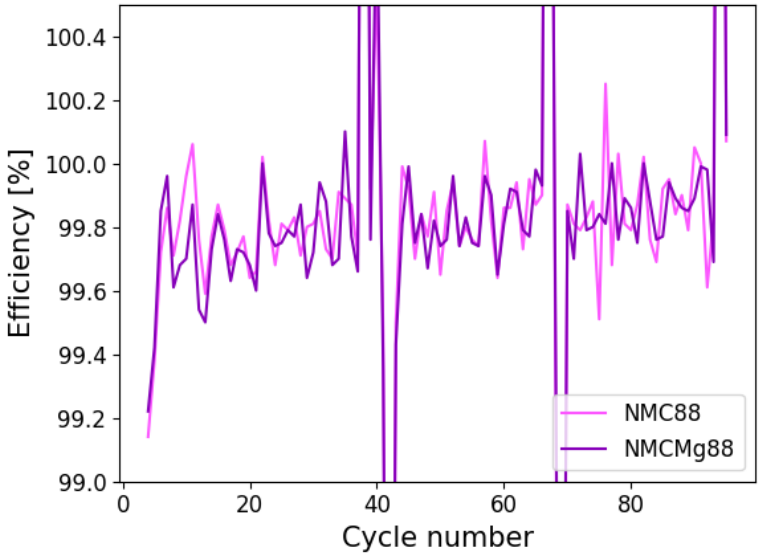

Figure 4.19: The coulombic efficiency of NMCMg88 and NMC88 cycled at C/3 for 95 cycles. At cycle 40 - 41, 67 - 68 and 94 - 95 the C-rate was C/10.

Figure 4.20 shows an extrapolation done on the discharge capacity plot in Figure 4.17 assuming constant decrease in discharge capacity. If the NMCMg88 and NMC88 were to cycle for a longer amount of time the discharge capacity would eventually drop to 80 % of the initial capacity, giving an estimated cycle life of 454 cycles and 564 cycles, respectively.

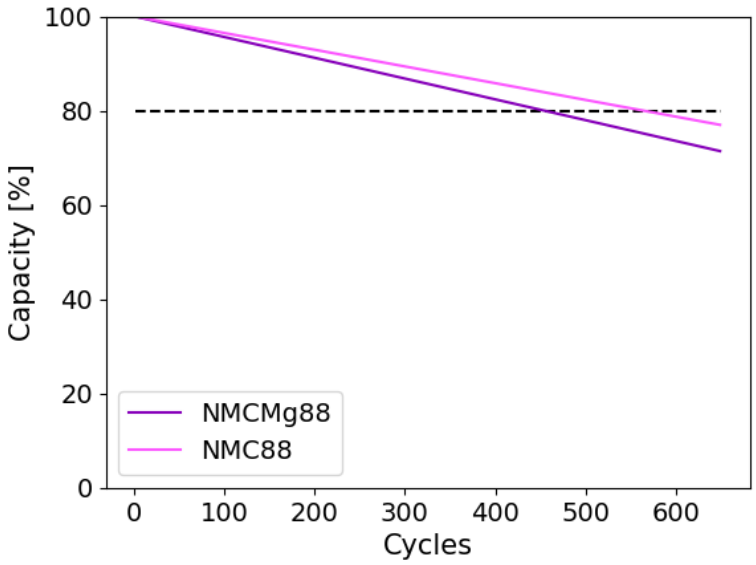

Figure 4.20: Extrapolated capacity retention for NMCMg88 and NMC88 assuming constant decrease in discharge capacity over an extended amount of cycles. Estimated cycle life of NMCMg88 and NMC88 is 454 and 564, respectively.

Nb Modification Investigation

In Figure 4.21 the first and second cycle of a) NMC88-Nb and b) NMC88-H graphite full cells cycled at C/20 is shown, where both cathodes show voltage plateaus around 4.1 V corresponding to the H2-H3 phase transition. The specific capacity, coulombic efficiency and irreversible loss of the first cycle are listed in Table 4.8

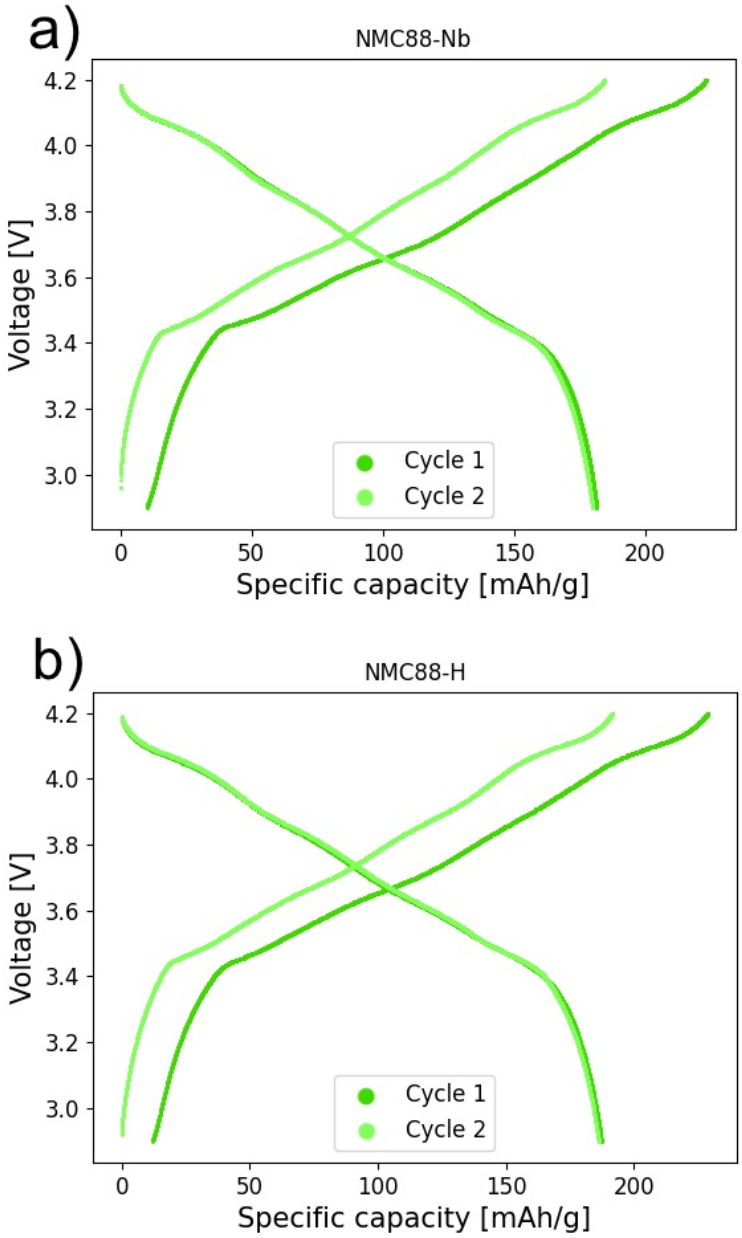

Figure 4.21: Voltage profile of the first and second cycle of a) NMC88-Nb and b) NMC88-H graphite full cells cycled at C/20. The cut-off voltages were set to 2.9 - 4.2 V.

The discharge capacity of NMC88-Nb and NMC88-H cycled at C/3 for 95 cycles is shown in Figure 4.22, illustrated as an average of a number of coin cells. Standard deviations between the individual coin cells are shown through error bars. Because of the error in the battery cycler, the formation cycles of these cells were also stopped at a lower cut-off voltage than what was programmed. The cells switched to C/10 at varying cycles also here and were restarted with an updated program after a cycler restart at cycle 40. The capacity retention of the NMC88-Nb and NMC88-H is given in Table 4.9.

Table 4.8: The first cycle capacity, coulombic efficiency and capacity loss for the Nb modified cathode and its reference, cycled at C/20.

Composition	Specific capacity [mAh/g]	Coulombic efficiency [%]	Irreversible capacity loss [mAh/g]
NMC88-Nb	177	80	35.8
NMC88-H	187	82	33.9

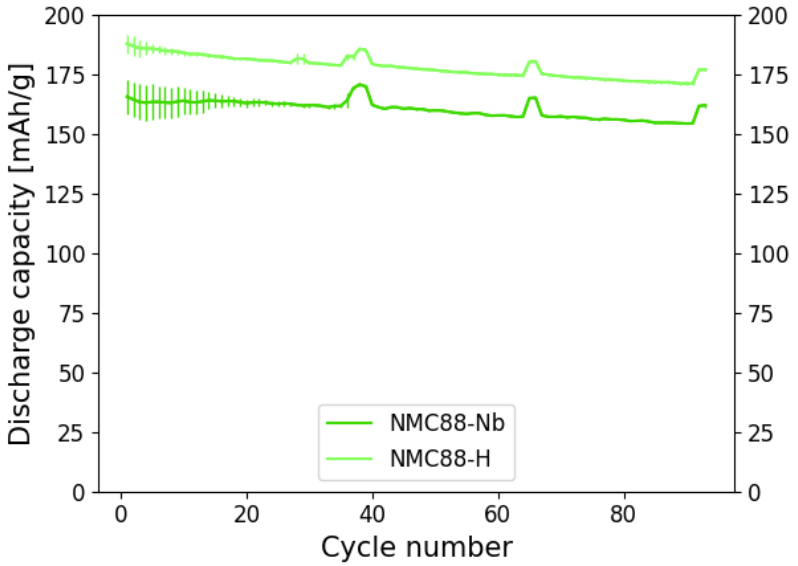

Figure 4.22: Discharge capacity for NMC88-Nb and NMC88-H, cycled at C/3 for 95 cycles. The C-rate was C/10 for two cycles for every 25th cycle, starting at cycle 38. The discharge capacity is given as an average of several coin cells with standard deviation shown with error bars.

Table 4.9: The discharge capacity retention of NMC88-Nb and NMC88-H.

Composition	1st cycle capacity at C/3 [mAh/g]	last cycle capacity at C/3 [mAh/g]	Retention [%] over 95 cycles
NMC88-Nb	166	154	93.2
NMC88-H	188	171	91.1

The discharge capacities of NMC88-Nb and NMC88-H at cycle 41, 68 and 95 cycled at C/10 is shown in Figure 4.18. At this C-rate both cathodes show similar capacity retention, though NMC88-Nb has a significantly lower discharge capacity in general.

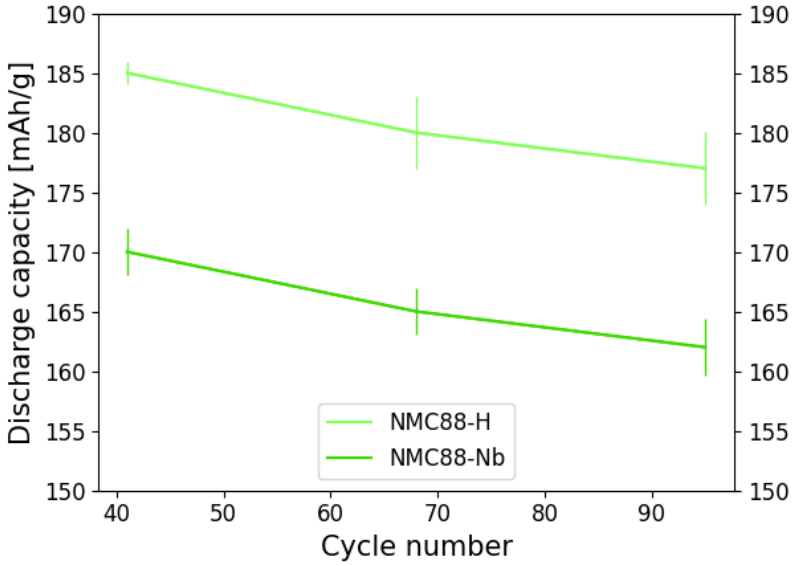

Figure 4.23: Discharge capacities for NMC88-Nb and NMC88-H at cycle 41, 68 and 95, cycled at C/10.

The coulombic efficiency of NMC88-Nb and NMC88-H cycled at C/3 for 95 cycles is shown in Figure 4.24. Both cathodes have similar efficiency and the expected increase and decrease in efficiency are present at the cycle ranges where the C-rate was adjusted to C/10.

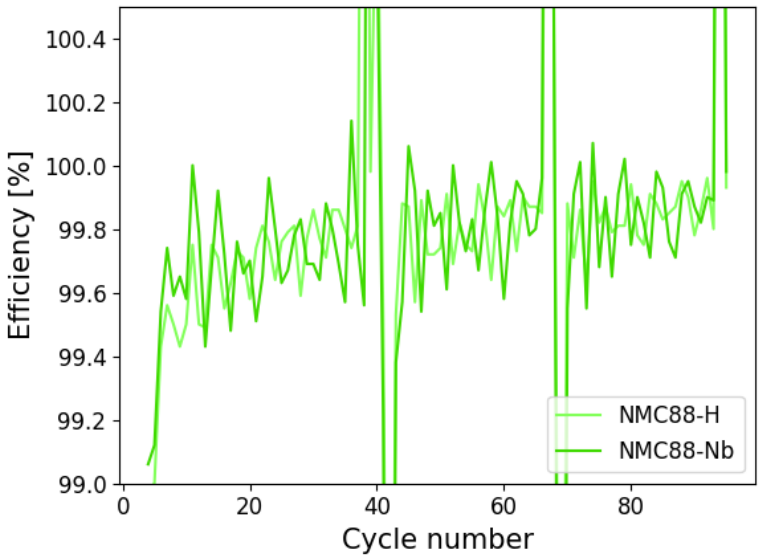

Figure 4.24: The coulombic efficiency of NMC88-Nb and NMC88-H cycled at C/3 for 95 cycles. The C-rate was adjusted to C/10 at cycle 40 - 41, 67 - 68 and 94 - 95.

An extrapolation of the discharge capacity for NMC88-Nb and NMC88-H is shown in Figure 4.25, where the estimated cycle life is 274 cycles for NMC88-Nb, and 209 cycles for NMC88-H. The extrapolation was done assuming a constant decrease in discharge capacity.

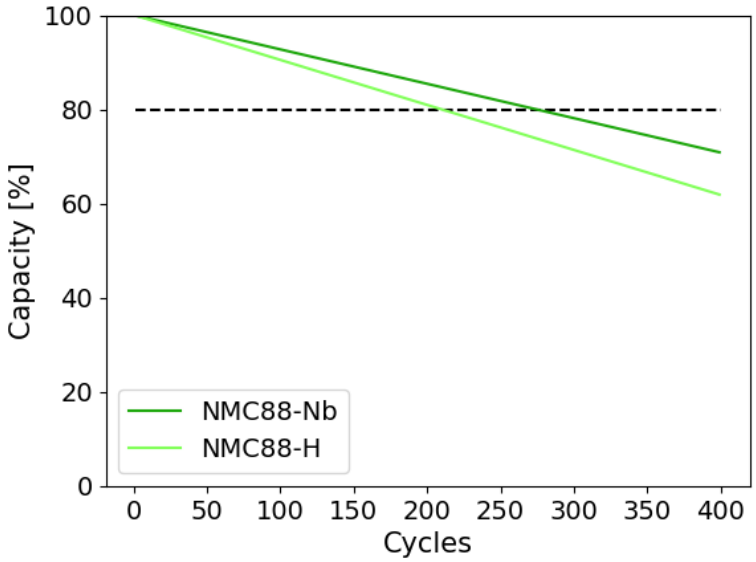

Figure 4.25: Extrapolated capacity retention for NMC88-Nb and NMC88-H, assuming constant decrease in discharge capacity over an extended amount of cycles. Estimated cycle life of NMC88-Nb and NMC88-H is 274 cycles and 209 cycles, respectively.

5 Discussion

5.1 Determination of Baseline Material

The annealing temperature of Ni-rich NMC materials is one of its many important parameters needing to be optimised to achieve the best performance. NMC88 has been shown to have an optimal annealing temperature at 750 °C, giving good and stable electrochemical results. When looking at NMC materials with 94 % Ni, it is important to take the annealing temperature into account to be able to benefit from the increased Ni-content. A temperature of 735 °C was investigated parallel to the 750 °C, to see which cathode gave the best electrochemical results. Different temperatures have been utilised when synthesising materials containing various amounts of Ni. The decision of using 735 °C was made due to earlier research proving that a temperature of 735 % C was optimal for materials with 90 % Ni[35]. The SEM analysis of the two powders did not show any visible differences, with both having primary particles of varying sizes below 1 µm agglomerated into bigger secondary particles. The XRD results also showed similarities in the X-ray diffractograms and the Rietveld refinement data, though the Ni-Li site disorder was significantly different. NMC94-735 had a much higher amount of Ni-Li disorder with 3.0 % compared to 1.7 % for NMC94-750. This indicates that the annealing temperature of 735 % C was not enough to form a defect-free structure, which is important because a high site disorder can limit the electrochemical performance of the batteries.

Looking at the initial capacity of the NMC94 cathodes cycled at C/10, the 750 cells give better results than the 735 cells. This is most likely a consequence of the high Ni-Li site disorder observed in the Rietveld refinements of the 735 cells, which causes more Li to become inactive when placed in the TM-layer. The cycling performance of the NMC94 cathodes showed an unexpected poor capacity retention when cycling for 100 cycles at C/2, compared to the results from previous work[38]. The half cells of NMC94-750 all had similar degradation throughout the 100 cycles when disregarding the test disturbances, indicating that the coin cell assembling was not the issue. Full cells with LTO as anode material were also made of the NMC94-750 cathode, which are expected to be more stable than half cells with Li. The LTO cells were more stable than the half cells, but the results still showed poor capacity retention compared to previous work[38]. Only two coin cells with the NMC94-735 cathode were able to cycle for the 100 cycles without too much disturbance, giving two very different results. The 735-1 coin cell seems to have a bit better capacity retention, though still not very good, and the 735-2 coin cell is closer to the cycling performance of NMC94-750 but with a lot of disturbances. Two more cells of the NMC94-735 cathode were able to cycle for 100 cycles despite having many disturbances and a bad connection to the coin cell holder. The discharge capacity retention of all four cells are shown in Figure A.12 in the Appendix, where the 735-1 and 735-3 cell showed a similar capacity retention trend, and the 735-2 and 735-4 cell showed a similar trend. From the calculated retention data the NMC94-735 cells

do give a better result, but because this is based on four cells with two different trends it is hard to conclude anything from the given data.

The coulombic efficiency was also investigated for the 750-2 half cell and the 735-1 half cell, where both cathodes showed a similar irreversible capacity loss in the first cycle. The 750 cell had a generally lower efficiency than the 735 cell after switching from C/10 to C/2, which is reflected in the capacity retention described earlier. The efficiency of the 750 cell is also lower than for the NMC94 cathode synthesised in [38], which had a minimum efficiency of 99.5 % at the same C-rate. However, the NMC94 cell in [38] was an LTO full cell, which in general has a better efficiency performance compared to half cells[43].

As the SEM imaging and XRD results do not indicate any impurities in the materials, a possible reason for the generally poor cycling stability could be rooted in the material synthesis process, as this is the common denominator for both materials. The air sensitivity of the material has been proven to be an issue, but NMC94 has been successfully synthesised and heat treated at 750 °C previously[38] using the same approach as in this experiment, with a much better performance. For this reason it is hard to come to a conclusion on which synthesis temperature is best. However, because the synthesis method was optimised for the NMC88 cathode, an increase in Ni-content would demand adjustments to the different synthesis parameters due to the increased instability of the material. Figure 5.1 shows the capacity degradation of one of the NMC94-750 LTO full cells cycled at C/2, compared to an NMC88 graphite full cell cycled at C/3. It is evident that the NMC88 has far better capacity retention when cycling for up to 100 cycles, disregarding the disturbances and increase in capacity due to C-rate adjustments. Materials with less Ni is expected to be more stable than those containing more Ni, which is the opposite of what Figure 5.1 shows. LTO should also generally provide a higher cycling stability compared to graphite[43], though in Figure 5.1 that is not the case. The significant difference in capacity retention for these two cathodes lead to the decision of continuing with NMC88 as baseline material for further investigations.

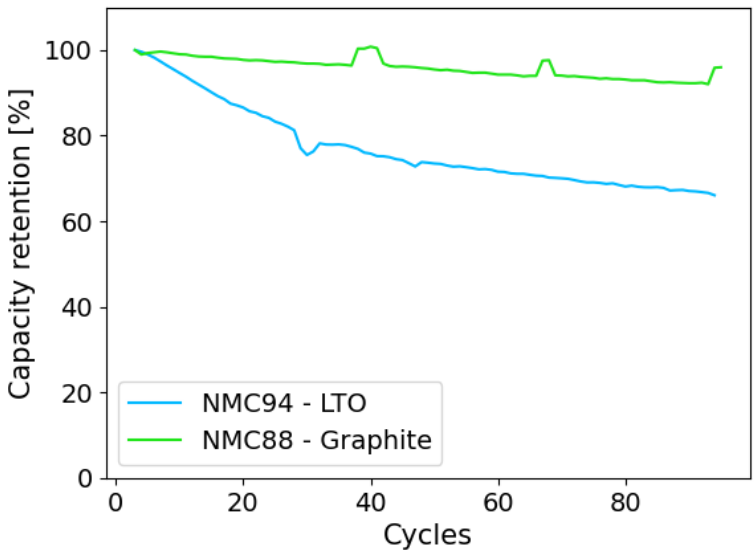

Figure 5.1: Discharge capacity of an NMC94-750 LTO full cell and an NMC88 graphite full cell cycled for 100 cycles. The LTO cell was cycled at C/2 and the graphite cell was cycled at C/3.

5.2 Mg Doping Studies

Doping NMC materials with Mg has been observed to improve the stability of the cathode giving the battery a longer cycle life. The structural instability of NMC cathodes with high Ni-content has made doping agents necessary for improved battery performance, and investigating a 1% Mg doping of the NMC88 material has provided some interesting results.

From the PSD results a monomodal size distribution was achieved for both the NMCMg88 and NMC88 reference, with agglomerate peaks of approximately the same sizes. The SEM imaging also showed similar results with primary particles of varying sizes below 1 µm for both cathode powders. When looking at the Rietveld refinements the data had little deviance between the two cathodes, and the Mg was confirmed to be preferably placed in the Li-layer, as was assumed from the results obtained in [38]. As a precaution for this assumption the NMCMg88 material was only added a 3 at% excess Li compared to 4 at%, as was added to the reference material. This was done to avoid additional excess Li from potentially forming surface species on the cathode, which could limit the battery performance.

From the first cycle at C/20 in Figure 4.16 both the Mg doped NMC88 and its reference have a very similar voltage profile. NMC88 has a slightly better specific capacity and coulombic efficiency, but the resulting irreversible capacity loss does not deviate from the NMCMg88 by much. The capacity retention over 95 cycles is very similar for both materials, with NMC88 being slightly better at 96.7 % compared to NMCMg88 at 95.9 %. The first 10 cycles of the cycle test show a decrease in discharge capacity for both NMCMg88 and

NMC88. This can be caused by incomplete wetting, due to the electrolyte being unevenly dispersed in the battery during assembly. A possible result of this is that the first cycle capacity at C/3 is higher for NMCMg88 than for NMC88, which is the opposite of what was observed for the first cycle at C/20. The increased standard deviation observable during the first 10 cycles of the cycling test is possibly due to the interruption in the formation cycles. This could be a result of the batteries trying to recover from being stopped at lower cut-off voltages than what they were programmed for. In Figure 4.18 the discharge capacities for the C/10 cycles are shown. Also at a low C-rate there is little deviance between the performance of the Mg doped material and the reference, where NMCMg88 has a slightly inferior discharge capacity here as well. The coulombic efficiency of the two cathodes does not show significant differences either, which has been the general observation in all aspects of the Mg doping investigations.

From these results it can be concluded that doping the NMC88 material with 1 % Mg does not improve the structural stability of the Ni-rich material, but causes slightly inferior electrochemical performance overall. This indicates that 1 % Mg doping is unnecessary for the NMC88 material, though it could be a beneficial doping for a higher Ni-content NMC cathode, such as the NMC94, due to the increasing instability with increased Ni-content. In [38] a 3 % Mg doping of NMC94 was investigated and a significant increase in stability was observed compared to the baseline NMC94. It did however cause lower specific capacity, which is why a 1 % Mg doping was investigated here.

5.3 Effects of Nb Modification and Post Annealing

The PSD results showed that a monomodal size distribution was achieved in the NMC88-1 powder before starting the Nb modification and post annealing treatment. In the SEM images the primary particle sizes of the NMC88-Nb and NMC88-H powder were of approximately the same sizes below 1 µm, which is expected as both powders originated from the same synthesis batch. The XRD results were also similar in both the X-ray diffractograms and the Rietveld refinement, but the Ni-Li site disorder showed a possible decreasing trend from the pre treated NMC88-1 powder to the NMC88-Nb and NMC88-H powder. Though the values are very similar and might have significant error.

The EDS analysis showed similar results when mapping different areas of the NMC88-Nb cathode powder. The mapping performed by Julian Tolchard in Figure 4.12 and Figure 4.13 indicates that there are traces of Nb everywhere in the powder sample, though a confirmation that the Nb has become a complete coating is not possible using this method. The varying results in the quantifications of the point detections shown in Table 4.4 and Table 4.5 are likely a result of EDS not being an optimal method for analysing powder samples with unknown morphology. When calculating how much Nb precursor was needed for the 2 wt% modification, the Nb was assumed to form a $LiNbO_3$ phase on the surface of the NMC88 particles. Assuming that none of the Nb formed this surface species but rather accumulated to Nb_2O_5 particles, the total amount of Nb_2O_5 produced would be 36 mg. The maximal amount

of $LiNbO_3$ possible to obtain is 40 mg. The Nb mapping in Figure 4.12 only revealed one hot spot of Nb in the powder sample, which indicates that most of the Nb was evenly distributed on the surface of the NMC88 powder. To confirm if the surface species are $LiNbO_3$ or other compounds further analysis methods must be utilised, for example transmission electron microscopy.

From the electrochemical results of the first cycle at C/20 the heat treated NMC88 reference had a higher specific capacity and coulombic efficiency compared to the Nb-modified cathode. This is the opposite of what has been observed in other research when modifying Ni-rich NMC materials with 2 wt% Nb[41]. An interesting observation is that the NMC88-H outperforms the specific capacity of the NMC88 reference used in the Mg doping, which becomes more prominent in the first cycle at C/3 in the cycling test. The difference between the two reference materials is only the post annealing treatment of the NMC88-H material which seems to have affected its electrochemical properties. Post annealing of NMC811 has been proven to enhance its electrochemical performance, though at temperatures above 400 °C oxygen vacancies were formed and an increase in Li-Ni site disorder was observed[44].

While achieving a higher specific capacity the NMC88-H simultaneously obtained a lower capacity retention compared to all the other NMC88 materials. The annealing temperature of 500 °C possibly caused increasing amounts of oxygen vacancies resulting in a less stable cathode structure. Another possibility is that the high capacity of the material made the structure less stable. For this reason it can be useful to compare the NMC88-Nb to NMC88 used as a reference in the previous section. The Nb modified material seems to be inferior to NMC88 when looking at the specific capacity and coulombic efficiency of the first cycle. However, the difference is small, and could be related to the formation of $LiNbO_3$ species on the cathode surface causing blockage of the Li-diffusion pathways.

The discharge capacity retention at C/3 over 95 cycles of the NMC88-Nb is also inferior to NMC88 with 93.2 % and 96.7 %, respectively. Another observation is that the NMC88-Nb has a larger standard deviation in the first 15 cycles, likely for the same reason as NMCMg88 and NMC88, that the battery is trying to recover from the interrupted formation cycles. The capacity retention of NMC88-H can also be interesting to look at here, because it is lower compared to all the others, at 91.1 %. As mentioned this is likely caused by a negative effect from the post annealing heat treatment, though since NMC88-Nb underwent the same treatment and still achieved a higher capacity retention, this could indicate that Nb does provide some structural stability to the cathode. There are a few factors here in need of further investigation to be able to understand the behaviour of the Nb modification better. One factor of significance is that the NMC88-H powder was not exposed to ethanol over time in the same way NMC88-Nb was when introduced to the Nb precursor, which could also have had an impact on the performance of the NMC88-Nb cathode. The C/10 cycles shown in Figure 4.23 show that both NMC88-Nb and NMC88-H seems to obtain a high discharge

capacity at low C-rates when cycled for 41, 68 and 95 cycles. The coulombic efficiency does not show any significant differences in performance either.

From the results obtained in this thesis the Nb modification did not achieve improved electrochemical performance and stability of the NMC88 cathode. The work of Fengxia Xin et al. [41] in which these investigations are based on showed improved specific capacity and coulombic efficiency of the first cycle, in addition to better capacity retention in the Nb modified NMC811 material. This research did however confirm an Nb coating on the material, and performing further analysis on NMC88-Nb may reveal the cause of the performance degradation to be related to the type and distribution of the Nb surface species formed on the powder. As an improvement in electrochemical performance has been observed in Nb modified Ni-rich NMC previously, further investigations should be done before concluding that the Nb does not increase the structural stability of the NMC88 material as is indicated by the findings in this thesis.

5.4 Cycle Life Analysis

To answer the question of whether the stability issues of Ni-rich NMC cathodes can be solved using Mg and Nb modification it is important to look at the capacity retention of the different materials for extended cycling. The cycle life the cathode is one of the main areas that the battery industry seeks to improve. An extrapolation was done for all four NMC88 materials to anticipate their cycle life for extended cycling, assuming a constant decrease in discharge capacity. All four extrapolations are shown in Figure 5.2. As indicated the NMC88 reference outperforms all the other cathodes with a cycle life of 564 cycles. This shows that neither of the Mg and Nb modification performed in this thesis was able to further stabilise the structure, with cycle lives of only 454 and 274 cycles. To put these numbers in perspective, the commercial NMC battery used in Teslas grid battery has been investigated to have a cycle life of 784 cycles[45]. For a coin cell to obtain a cycle life of more than 500 cycles is a very good result, however the real performance of the batteries will deviate from the linear approximation which is why a conclusion can not be drawn from these results.

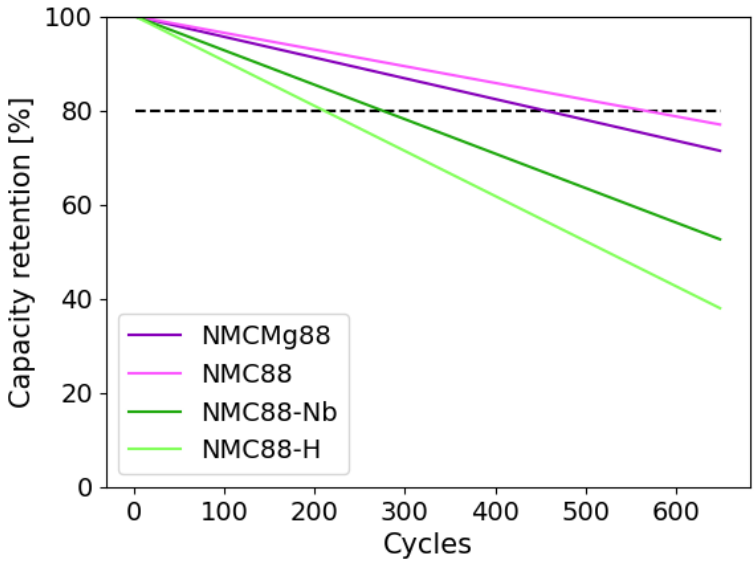

Figure 5.2: Extrapolated capacity retention for all four NMC88 cathodes assuming constant decrease in discharge capacity for extended cycling of the cells. The estimated cycle life of NMCMg88, NMC88, NMC88-Nb and NMC88-H is 454, 564, 274 and 209 cycles, respectively.

6 Conclusion

The Ni-rich layered oxides NMC94, NMC88, NMCMg88 and Nb modified NMC88 were successfully synthesised by an oxalic acid co-precipitation method. Utilising the two different temperatures 735 °C and 750 °C in annealing of the NMC94 cathode powder resulted in a generally poor cycling performance for both cathodes, though the 735 cathodes had slightly better capacity retention. The specific capacity of the 735 cathodes was however not as high as for the 750 cathodes. The cause for the general instability during cycling is possibly related to the synthesis of the material, as the SEM and XRD results indicated a phase pure material with no impurities. This was also the process done equally for both cathodes before the annealing, making it more likely to be the source of the instability affecting both materials. Because the synthesis method was optimised for an NMC88 cathode material, the higher Ni-content in NMC94 would need adjustments to the synthesis parameters due to the increased instability compared to NMC88. A comparison of discharge capacity retention of an NMC94-750 full cell and an NMC88 full cell revealed much higher stability in the NMC88 material, leading to the decision of using NMC88 as baseline material for further investigations.

The NMCMg88 cathode had an overall similar performance to the reference material, but with a slightly lower specific capacity and capacity retention, indicating that 1 % Mg does not provide any additional stabilisation to the Ni-rich structure. The low specific capacity of the NMCMg88 is likely related to Mg being favourably placed in the Li-layer of the structure, which causes more Li to become inactive. Because previous work[38] showed that 3 % Mg doping was too much as the capacity was significantly reduced despite the high capacity retention, the results here indicate that 1 % Mg is insufficient for stabilisation of the Ni-rich NMC structure.

The EDS analysis of NMC88-Nb revealed that the modification method was able to distribute the Nb evenly through the powder with minimal accumulation, though it was not possible to confirm that a coating of $LiNbO_3$ was successfully made through the analysis methods performed in this thesis. The electrochemical results of NMC88-Nb showed a lower specific capacity and improved cycling stability compared to NMC88-H. The post annealing did however affect the electrochemical performance of the NMC88-H, providing a higher specific capacity and lower capacity retention compared to the untreated NMC88 used as reference material in the Mg investigations. Comparing the NMC88-Nb to NMC88 is therefore more relevant, where the Nb modified cathode is inferior in electrochemical performance overall. An important observation is that the NMC88-Nb had also undergone the same post annealing treatment that provided such a poor capacity retention to NMC88-H, meaning that the higher capacity retention of NMC88-Nb could indicate that Nb modifying possesses some stabilising properties. Nb has been observed to provide stability and enhanced electrochemical performance in the work performed by Fengxia Xin [41], and a possible

cause for the poor performance observed in this thesis is that the Nb was not able to form a complete $LiNbO_3$ coating on the NMC88 powder.

Lastly, the cycle life extrapolations performed on all powders revealed that none of the Mg or Nb modified cathodes were able to stabilise the Ni-rich NMC88 structure, where the reference NMC88 showed the longest cycle life of 564 cycles. For a coin cell to have an estimated cycle life of more than 500 cycles is a very good result, though it is important to mention that the capacity retention extrapolation is only indicative as a deviation from the linear approximation is expected. Adjustments to modification amounts and methods or possibly replacing the modifying agents with other candidates are necessary to obtain improved structural stability of the NMC88 structure. These findings can hopefully contribute to further development in stabilisation of Ni-rich layered oxide cathodes for Li-ion batteries.

7 Further Work

The previous work performed in [38] showed increased capacity retention when doping NMC94 with 3 % Mg, but additionally a large decrease in specific capacity was obtained. From this a 1 % Mg doping was suggested as an interesting doping amount for the NMC94 cathode, which was the initial plan to explore in this master thesis. As this was not completed due to change in baseline material here, it would be interesting to make a new attempt at 1 % Mg doping of the NMC94 structure. Synthesising a stable NMC94 structure on its own would be the first step, to see if the stable cycling progression observed in previous work [38] is attainable. The next step would be doping the NMC94 structure with 1 % Mg to investigate if this would have an additional stabilising effect on the cycling performance.

The Nb modification is also an interesting research topic for further work. Determining if the decrease in specific capacity is related to the ethanol exposure during the modifying process, or to the Nb modification itself could be useful. It could also be interesting to see if increasing the modifying temperature to 700 °C would improve the electrochemical performance. The temperature determines if the Nb becomes a coating or if it diffuses into the structure, and it could be beneficial to investigate if doping or coating is the best way to stabilise the Ni-rich layered oxide structure. It would also be useful to determine if an incomplete $LiNbO_3$ coating causes degradation in electrochemical performance.

Lastly, it could be worth looking into is the increase in capacity for NMC88 when going through a post annealing process. Heat treating the cathode powder at 500 °C for three hours seemed to have a significant increase in capacity for the NMC88 reference for the Nb modified material, as opposed to the NMC88 reference for NMCMg88. The two powders also originated from two different synthesis batches, which is another possible source of the improved first cycle performance of NMC88. Investigating if any of these two processes have affected the first cycle performance of the NMC88 material, could be interesting.

References

[1] Florian Egli et al. “A dynamic analysis of financing conditions for renewable energy technologies”. In: *Nature Energy* 3 (2018), pp. 1084–1092.

[2] Jaephil Cho et al. “Commercial and research battery technologies for electrical energy storage applications”. In: *Progress in Energy and Combustion Science* 48 (2015), pp. 84–101.

[3] Mengyao Lu et al. “Research progress on power battery cooling technology for electric vehicles”. In: *Energy Storage* 27 (2020), pp. 101–155.

[4] Martin Winter et al. “Before Li Ion Batteries”. In: *Chemical Reviews* 118 (2018), pp. 11433–11456.

[5] Chiara Busà et al. “The effects of ambient storage conditions on the structural and electrochemical properties of NMC-811 cathodes for Li-ion batteries”. In: *Electrochimica Acta* 366 (2020), p. 137358.

[6] Hongfei Zheng et al. “Recent developments and challenges of Li-rich Mn-based cathode materials for high-energy lithium-ion batteries”. In: *Materials Today Energy* 18 (2020), p. 100518.

[7] Dong Ren et al. “There and Back Again — The Journey of $LiNiO_2$ as a Cathode Active Material”. In: *Angewandte Chemie International Edition* 58.31 (2019), pp. 10434–10458.

[8] Yong Lu et al. “Recent advances in Ni-rich layered oxide particle materials for lithium-ion batteries”. In: *Particuology* 53 (2020), pp. 1–11.

[9] Fengxia Xin et al. “What is the Role of Nb in Nickel-Rich Layered Oxide Cathodes for Lithium-Ion Batteries?” In: *American Chemical Society* 6.4 (2021), pp. 1377–1382.

[10] Naoki Nitta et al. “Li-ion battery materials: present and future”. In: *Materials Today* 18.5 (2015), pp. 252–264.

[11] Irmgard Hedwig Buchberger. *Electrochemical and structural investigations on lithium-ion battery materials and related degradation processes*. 2016. URL: `https://d-nb.info/1113749180/34`. (Accessed: 14.12.2021).

[12] Christian Julien et al. *Lithium Batteries*. Springer, 2016.

[13] John B. Goodenough et al. “Challenges for Rechargeable Li Batteries”. In: *American Chemical Society* 22.3 (2009), pp. 587–603.

[14] Pekka Peljo et al. “Electrochemical potential window of battery electrolytes: the HOMO–LUMO misconception”. In: *Energy and Environmental Science* 11 (2018), p. 2306.

[15] Satu Kristiina Heiskanen et al. “Generation and Evolution of the Solid Electrolyte Interphase of Lithium-Ion Batteries”. In: *Joule* 10.3 (2019), pp. 2322–2333.

[16] Erik Björklund et al. “How the Negative Electrode Influences Interfacial and Electrochemical Properties of $LiNi_{1/3}Co_{1/3}Mn_{1/3}O_2$ Cathodes in Li-Ion Batteries”. In: *The Electrochemical Society* 164.13 (2017), A3054.

[17] Subrahmanyam Goriparti et al. “Review on recent progress of nanostructured anode materials for Li-ion batteries”. In: *Power Sources* 257 (2014), pp. 421–443.

[18] Da Li et al. “Synthesis of $Li_4Ti_5O_{12}$ with theoretical capacity in Li_2CO_3-ammonia-ballmilling system”. In: *Materials Research Bulletin* 114 (2019), pp. 177–183.

[19] Ali Eftekhari. “Low voltage anode materials for lithium-ion batteries”. In: *Energy Storage Materials* 7 (2017), pp. 157–180.

[20] Jeffrey W.Fergus. “Recent developments in cathode materials for lithium ion batteries”. In: *Power Sources* 195.4 (2010), pp. 939–954.

[21] M. Saiful Islam et al. “Lithium and sodium battery cathode materials: computational insights into voltage, diffusion and nanostructural properties”. In: *Chemical Society Reviews* 43 (2014), pp. 185–204.

[22] C. Delmas et al. “Structural classification and properties of the layered oxides”. In: *Physica B+C* 99.1-4 (1980), pp. 81–85.

[23] M. M. Thackeray. “Structural Considerations of Layered and Spinel Lithiated Oxides for Lithium Ion Batteries”. In: *The Electrochemical Society* 142.8 (1995), p. 2558.

[24] John Campbell. *Why Cobalt Mining in the DRC Needs Urgent Attention*. 2020. URL: `cfr.org/blog/why-cobalt-mining-drc-needs-urgent-attention`. (Accessed: 14.12.2021).

[25] Ho-Hyun Sun et al. “Impact of Microcrack Generation and Surface Degradation on a Nickel-Rich Layered $Li[Ni_{0.9}Co_{0.05}Mn_{0.05}]O_2$ Cathode for Lithium-Ion Batteries”. In: *American Chemical Society* 29.19 (2017), pp. 8486–8493.

[26] Hong Sun et al. “Electronic Structure and Comparative Properties of $LiNi_xMn_yCo_zO_2$ Cathode Materials”. In: *American Chemical Society* 121.11 (2017), pp. 6002–6010.

[27] Glenn C. Mather et al. “A review of cation-ordered rock salt superstructure oxides”. In: *Materials Chemistry* 10 (2000), pp. 2219–2230.

[28] Wangda Li et al. “High-Nickel NMA: A Cobalt-Free Alternative to NMC and NCA Cathodes for Lithium-Ion Batteries”. In: *Advanced Materials* 32.33 (2020), p. 2002718.

[29] Zhen Chen et al. “Manganese phosphate coated $Li[Ni_{0.6}Co_{0.2}Mn_{0.2}]O_2$ cathode material: Towards superior cycling stability at elevated temperature and high voltage”. In: *Power Sources* 402 (2018), pp. 263–271.

[30] Seong-Min Bak et al. “Structural Changes and Thermal Stability of Charged $LiNi_xMn_yCo_zO_2$ Cathode Materials Studied by Combined In Situ Time-Resolved XRD and Mass Spectroscopy”. In: *American Chemical Society* 6.24 (2014), pp. 22594–22601.

[31] Sooyeon Hwang et al. “Investigation of Changes in the Surface Structure of $Li_xNi_{0.8}Co_{0.15}Al_{0.05}O_2$ Cathode Materials Induced by the Initial Charge”. In: *American Chemical Society* 26.2 (2014), pp. 1084–1092.

[32] Roland Jung et al. “Effect of Ambient Storage on the Degradation of Ni-Rich Positive Electrode Materials (NMC811) for Li-Ion Batteries”. In: *The Electrochemical Society* 165.2 (2018), A132–A141.

[33] Toru Hatsukade et al. “Origin of Carbon Dioxide Evolved during Cycling of Nickel-Rich Layered NCM Cathodes”. In: *American Chemical Society* 10.45 (2018), pp. 38892–38899.

[34] Chiara Busà et al. “The effects of ambient storage conditions on the structural and electrochemical properties of NMC-811 cathodes for Li-ion batteries”. In: *Electrochimica Acta* 366 (2021), p. 137358.

[35] Hongyang Li et al. “Is Cobalt Needed in Ni-Rich Positive Electrode Materials for Lithium Ion Batteries?” In: *The Electrochemical Society* 166.4 (2019), A429–A439.

[36] Kyoungmin Min et al. “A first-principles study of the preventive effects of Al and Mg doping on the degradation in $LiNi_{0.8}Co_{0.1}Mn_{0.1}O_2$ cathode materials”. In: *Physical Chemistry Chemical Physics* 19 (2016), pp. 1762–1769.

[37] Hyung-Joo Noh et al. “Comparison of the structural and electrochemical properties of layered $Li[Ni_xCo_yMn_z]O_2$ (x = 1/3, 0.5, 0.6, 0.7, 0.8 and 0.85) cathode material for lithium-ion batteries”. In: *Power Sources* 233 (2013), pp. 121–130.

[38] Siri Andersen. *Towards Cobalt Free Ultra-High Nickel Layered Oxide Cathodes For Li-ion Batteries*. Department of Materials Science, Norwegian University of Science and Technology, 2021.

[39] Wangda Li et al. “Collapse of $LiNi_{1-x-y}Co_xMn_yO_2$ Lattice at Deep Charge Irrespective of Nickel Content in Lithium-Ion Batteries”. In: *American Chemical Society* 141.13 (2019), pp. 5097–5101.

[40] Chong S. Yoon et al. “Structural Stability of $LiNiO_2$ Cycled above 4.2 V”. In: *ACS Energy Letters* 2.5 (2017), pp. 1150–1155.

[41] Fengxia Xin et al. “Li–Nb–O Coating/Substitution Enhances the Electrochemical Performance of the $LiNi_{0.8}Mn_{0.1}Co_{0.1}O_2$ (NMC 811) Cathode”. In: *American Chemical Society* 11.38 (2019), pp. 34889–34894.

[42] Harald Norrud Pollen et al. “A single-pot co-precipitation synthesis route for Ni-rich layered oxide materials with high cycling stability”. In: *Journal name under consideration* (To be submitted 2022).

[43] Erik Bjorklund et al. “How the Negative Electrode Influences Interfacial and Electrochemical Properties of LiNi1/3Co1/3Mn1/3O2 Cathodes in Li-Ion Batteries”. In: *The Electrochemical Society* 164.13 (2017), A3054–A3059.

[44] Ting Wang et al. “Tuning the Li/Ni Disorder of the NMC811 Cathode by Thermally Driven Competition between Lattice Ordering and Structure Decomposition”. In: *Physical Chemistry* 124 (2020), pp. 5600–5607.

[45] Fangfang Yang et al. “A study of the relationship between coulombic efficiency and capacity degradation of commercial lithium-ion batteries”. In: *Energy* 145 (2018), pp. 486–495.

A Appendix

A SEM

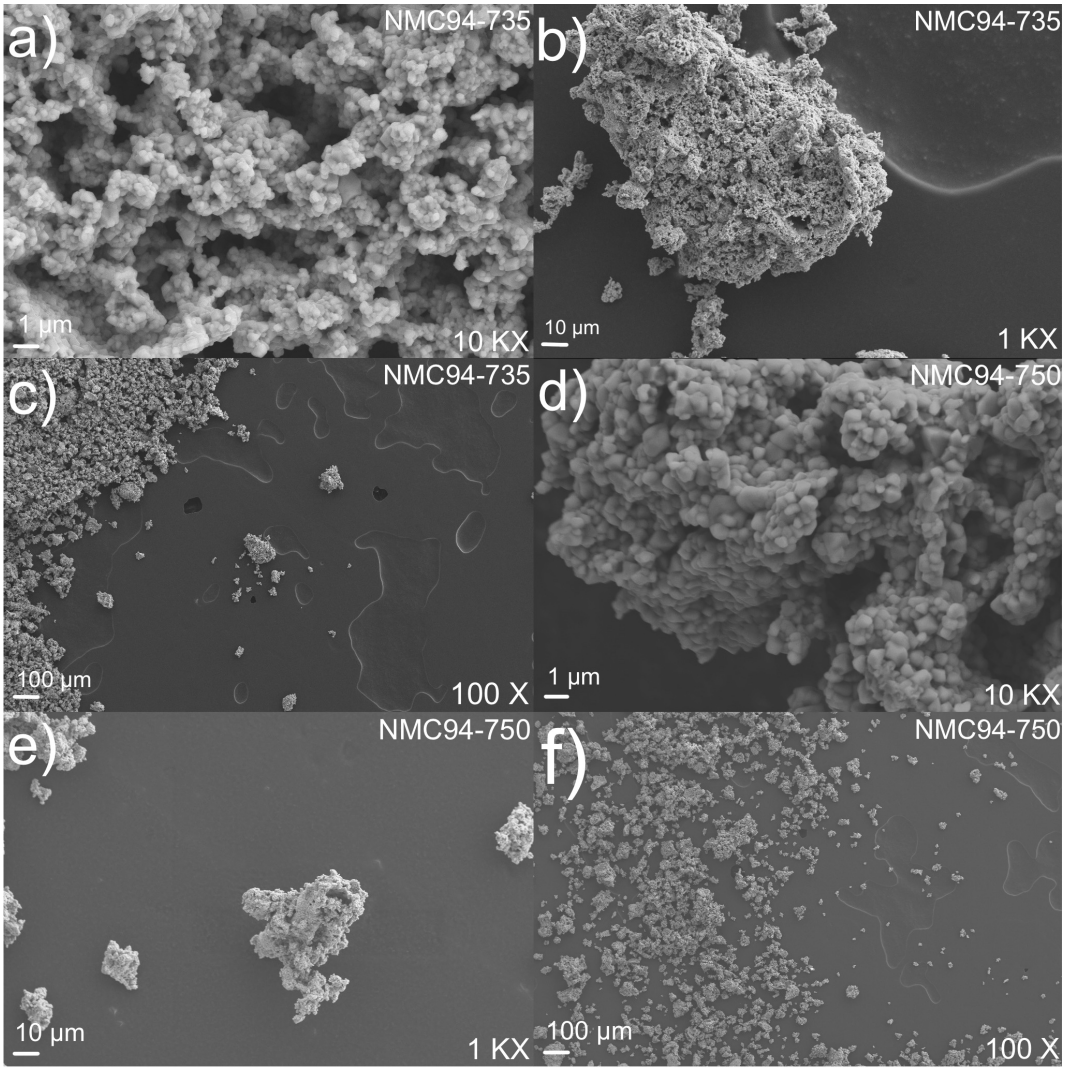

Figure A.1: SEM micrographs of NMC94-735 taken at magnification a) 10 kX, b) 1 kX and c) 100 X, and NMC94-750 taken at magnification d) 10 kX, e) 1 kX and f) 100 X.

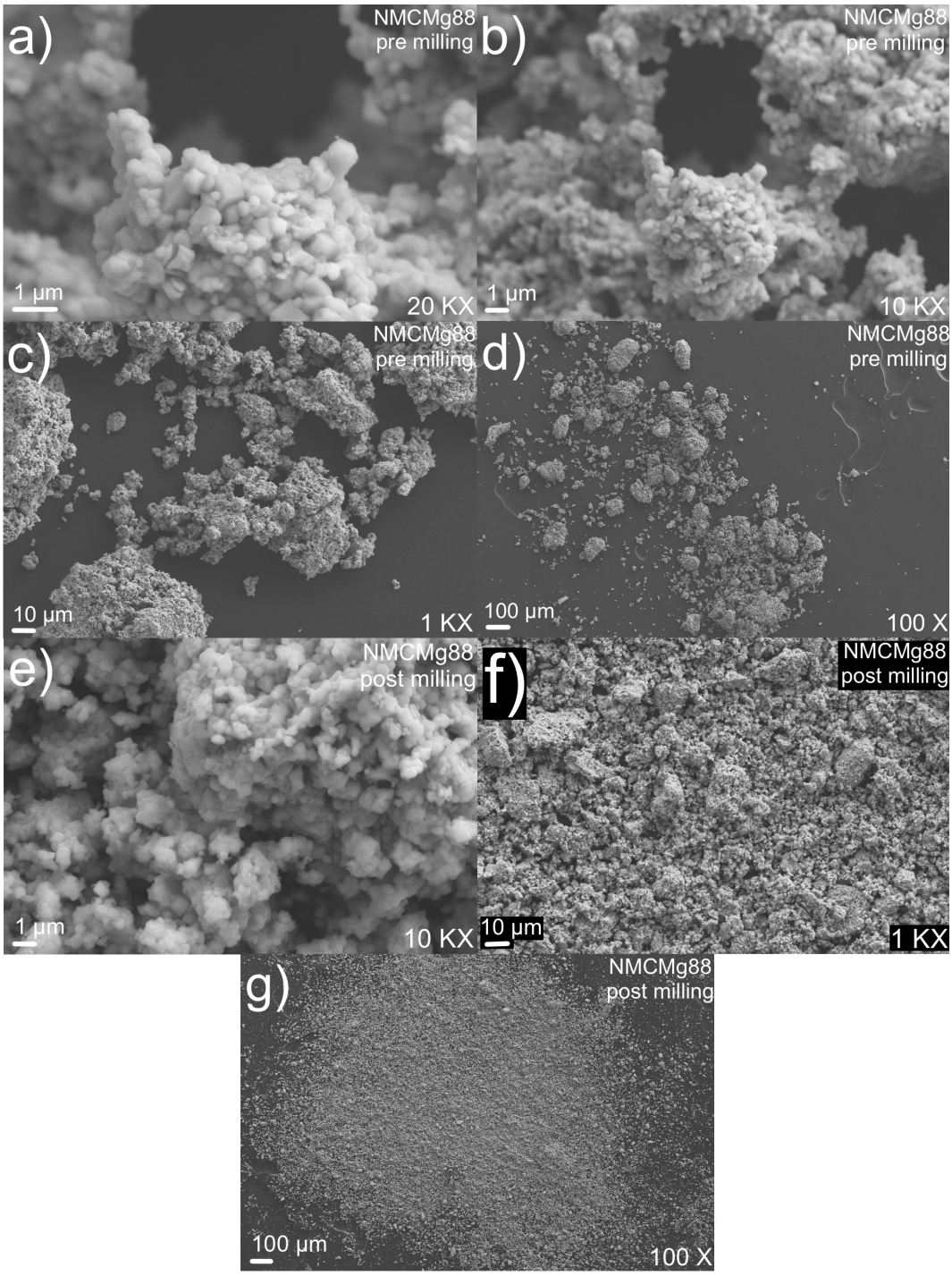

Figure A.2: SEM micrographs of NMCMg88 pre milling taken at a) 20 kX, b) 10 kX, c) 1 kX and d) 100 X, and post milling taken at magnification e) 10 kX, f) 1 kX and g) 100 X.

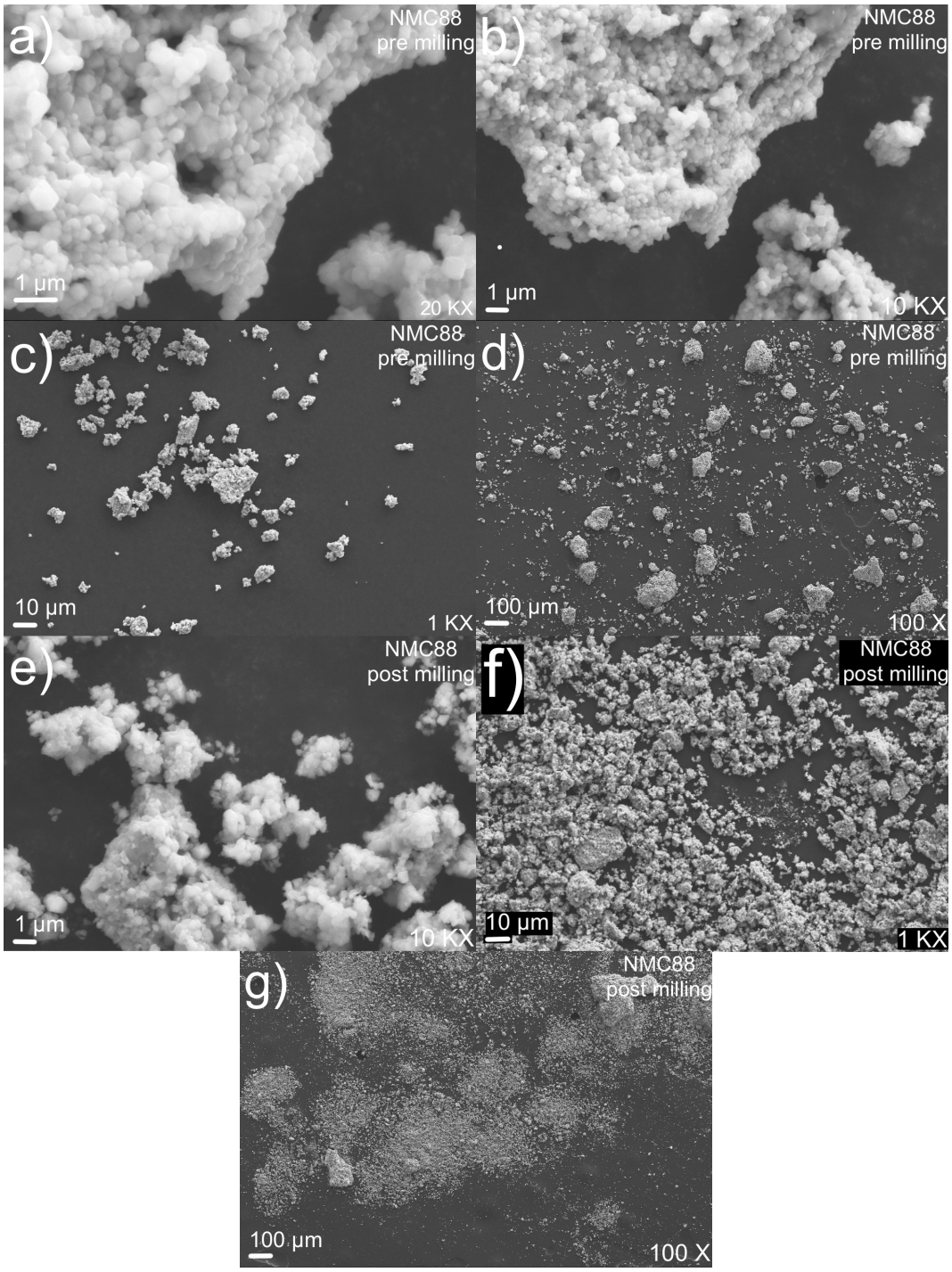

Figure A.3: SEM micrographs of NMC88 pre milling taken at a) 20 kX, b) 10 kX, c) 1 kX and d) 100 X, and post milling taken at magnification e) 10 kX, f) 1 kX and g) 100 X.

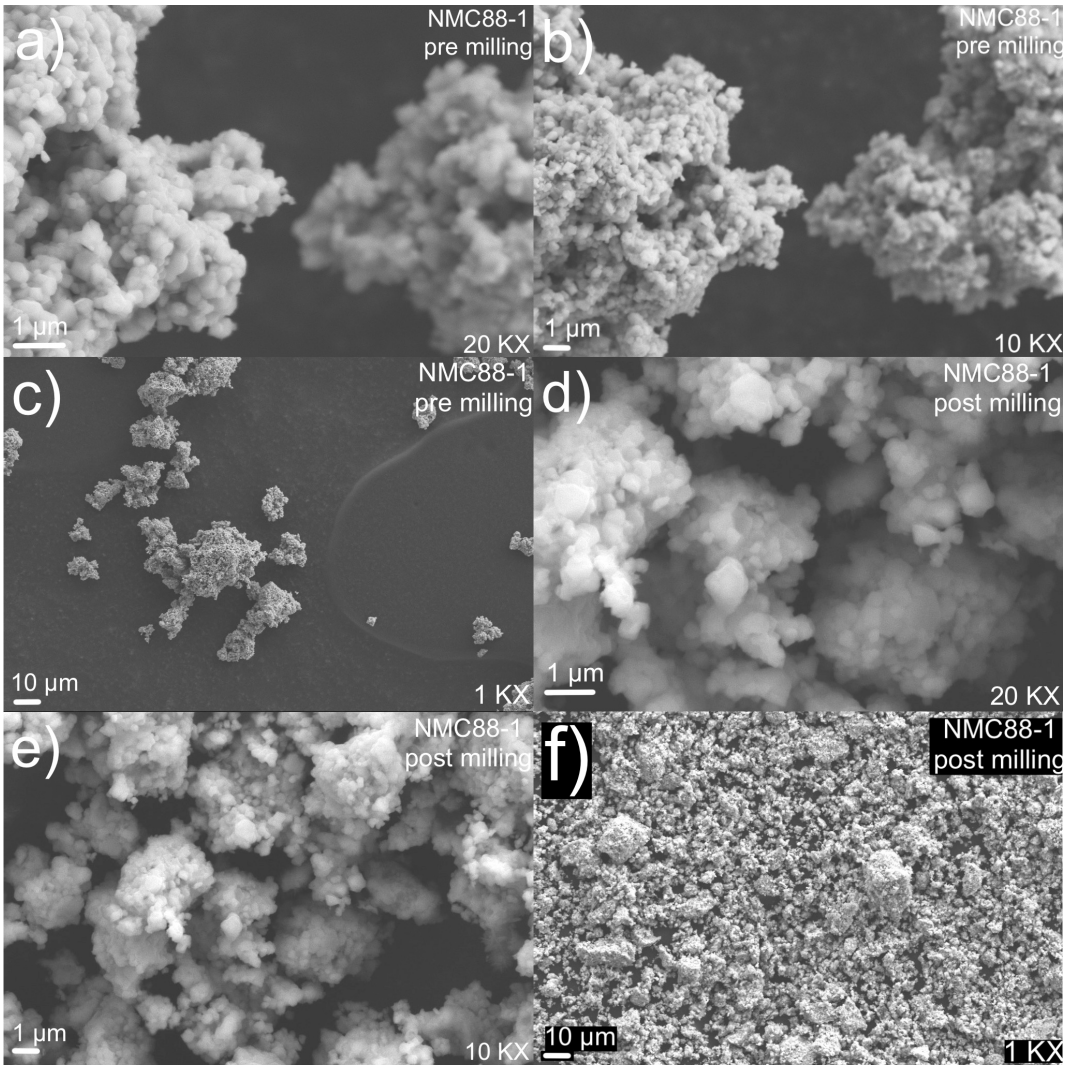

Figure A.4: SEM micrographs of NMC88-1 pre milling taken at a) 20 kX, b) 10 kX and c) 1 kX, and post milling taken at magnification d) 20 kX, e) 10 kX and f) 1 kX.

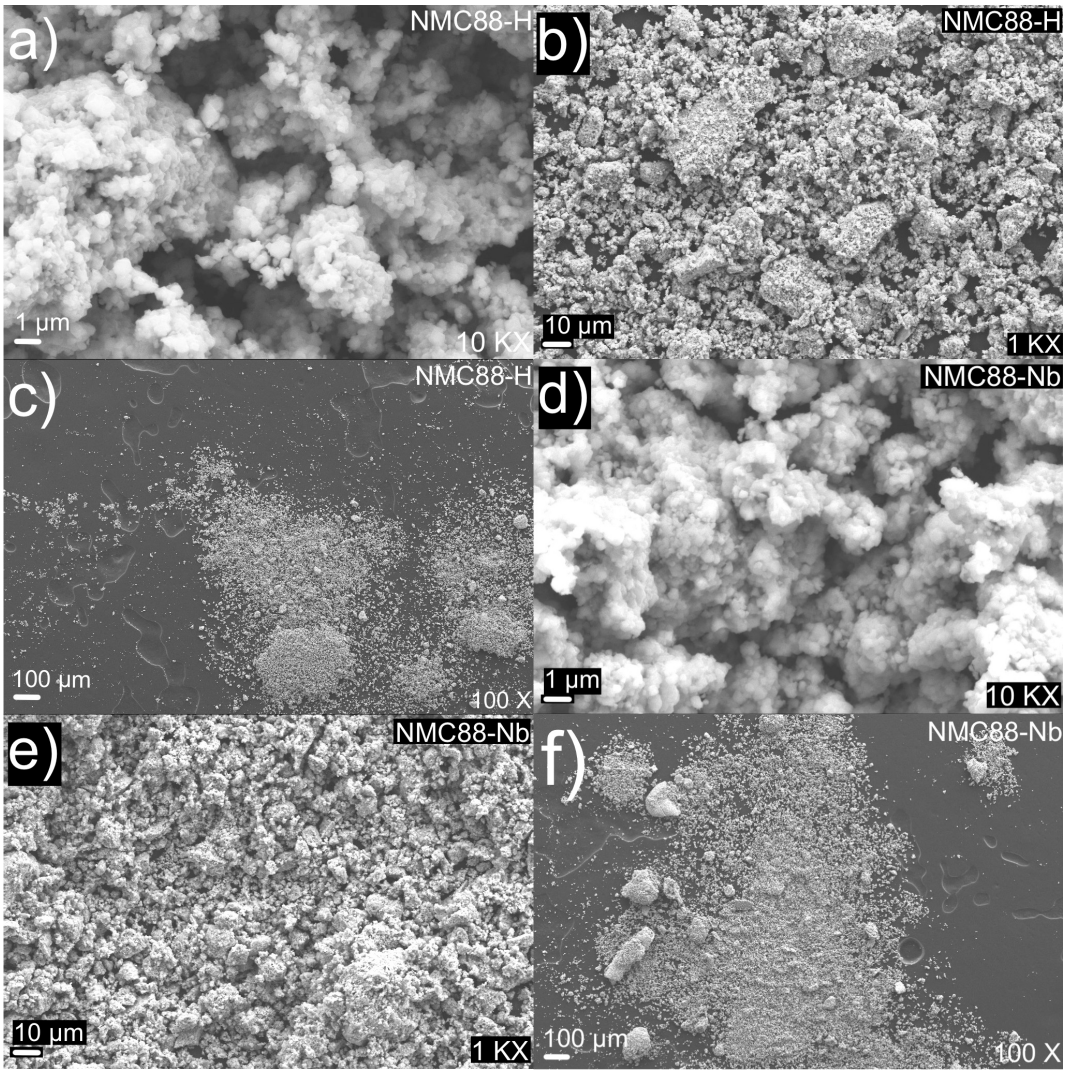

Figure A.5: SEM micrographs of NMC88-H taken at magnification a) 10 kX, b) 1 kX and c) 100 X, and NMC88-Nb taken at magnification d) 10 kX, e) 1 kX and f) 100 X.

B EDS

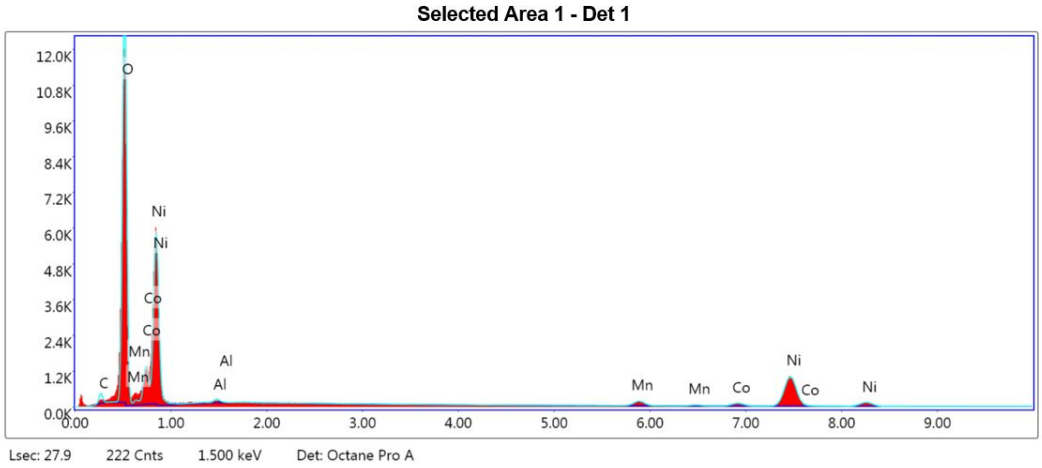

Figure A.6: EDS spectra of area 1 in the powder sample of NMC88-Nb.

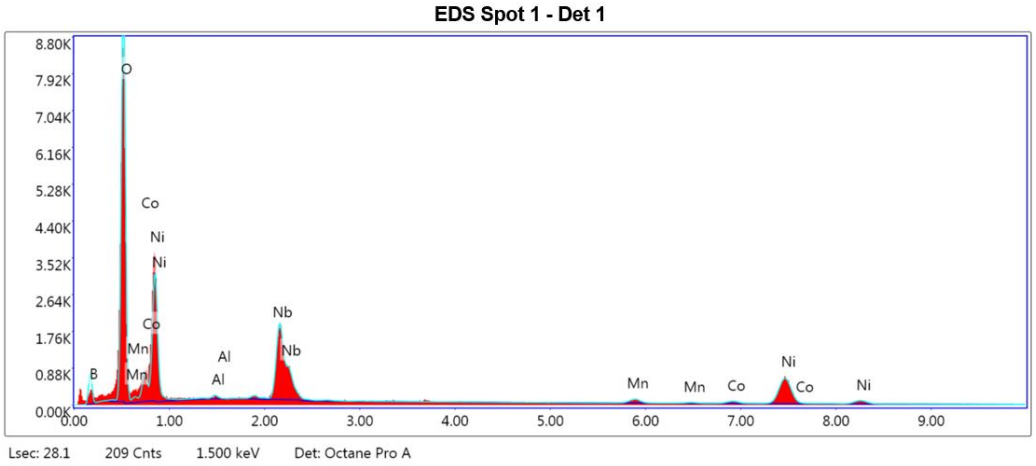

Figure A.7: EDS spectra of spot 1 in the powder sample of NMC88-Nb.

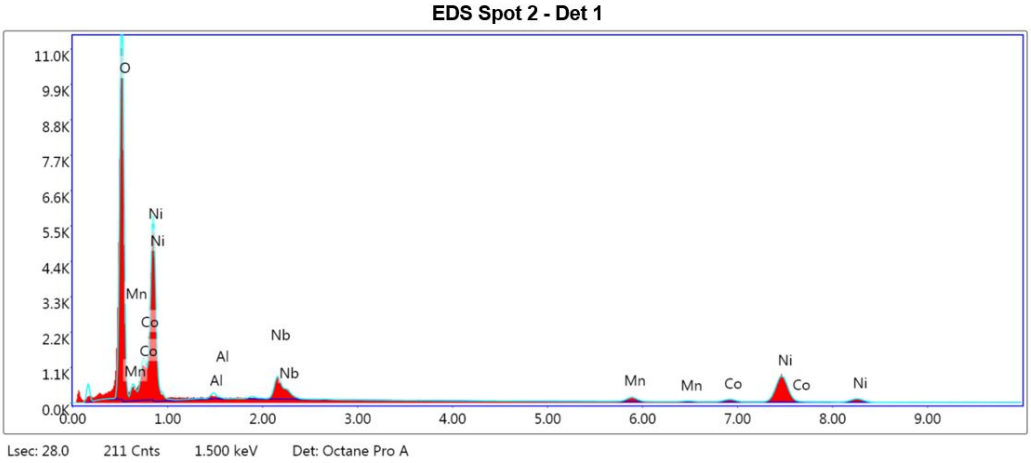

Figure A.8: EDS spectra of spot 2 in the powder sample of NMC88-Nb.

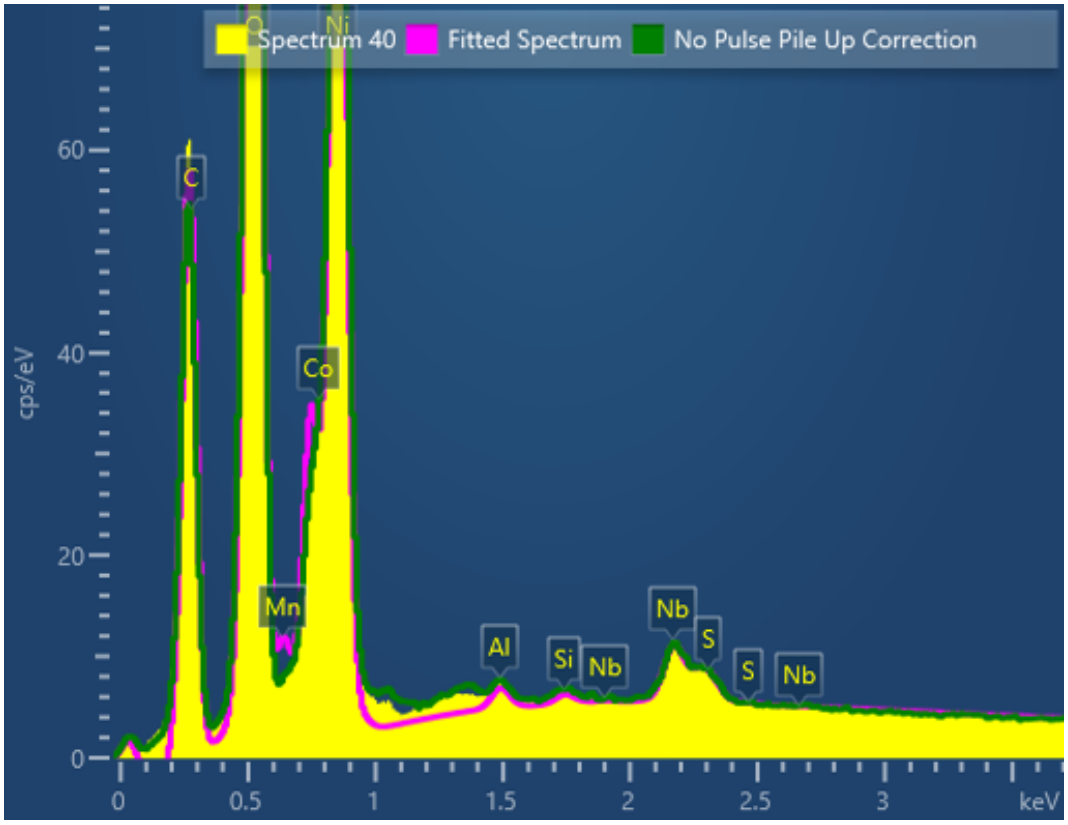

Figure A.9: EDS spectra of spectra 40 in the powder sample of NMC88-Nb performed by Julian Tolchard.

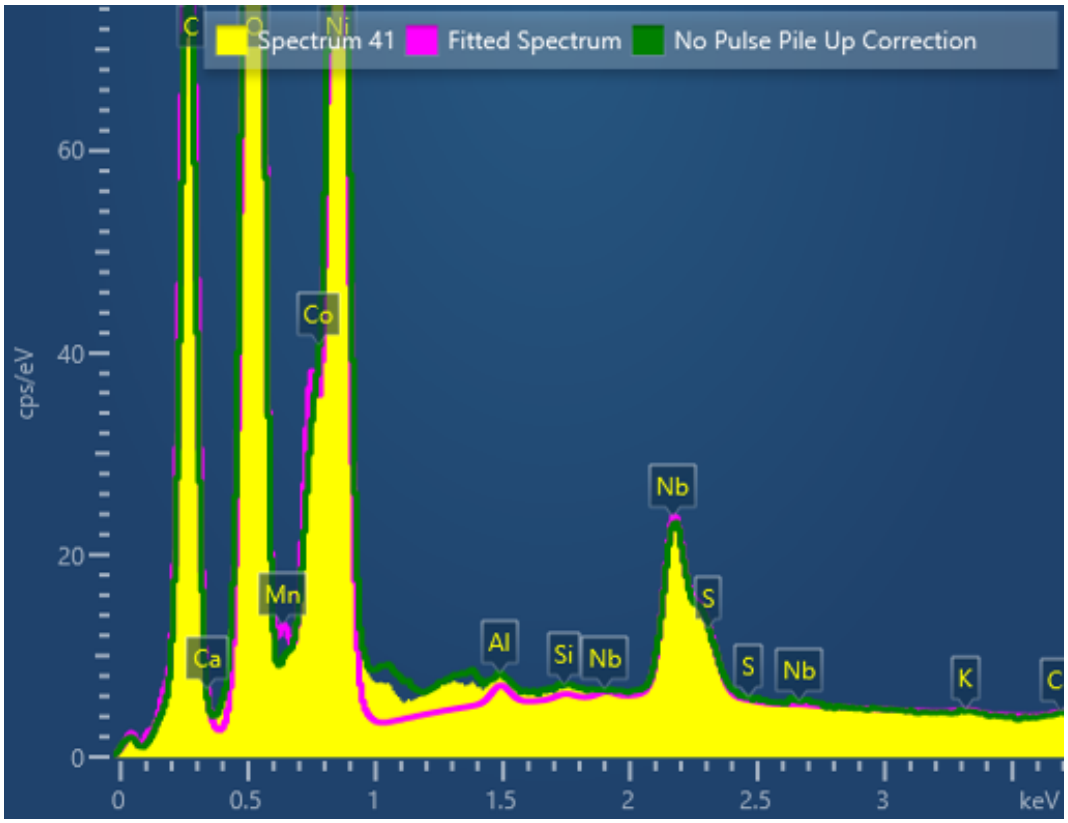

Figure A.10: EDS spectra of spectra 41 in the powder sample of NMC88-Nb performed by Julian Tolchard.

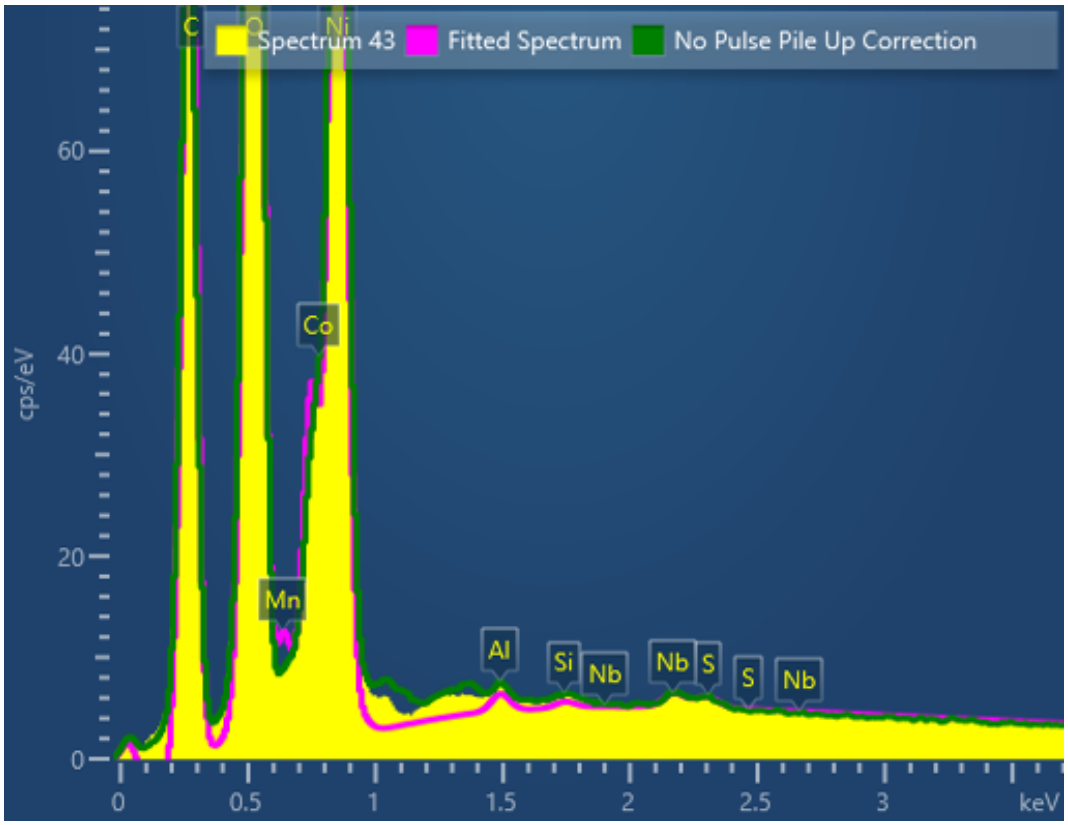

Figure A.11: EDS spectra of spectra 43 in the powder sample of NMC88-Nb performed by Julian Tolchard.

C Battery Testing

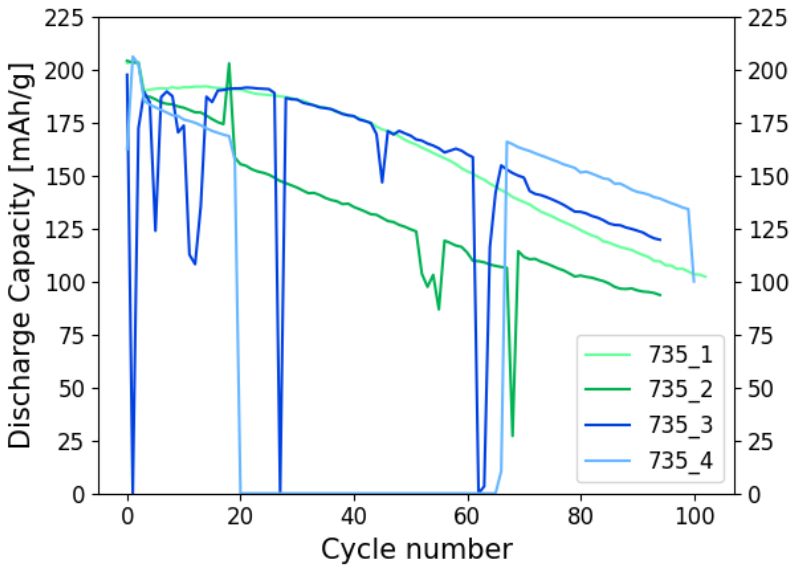

Figure A.12: Discharge capacity of all four NMC94-735 cells cycled for 100 cycles at C/2.

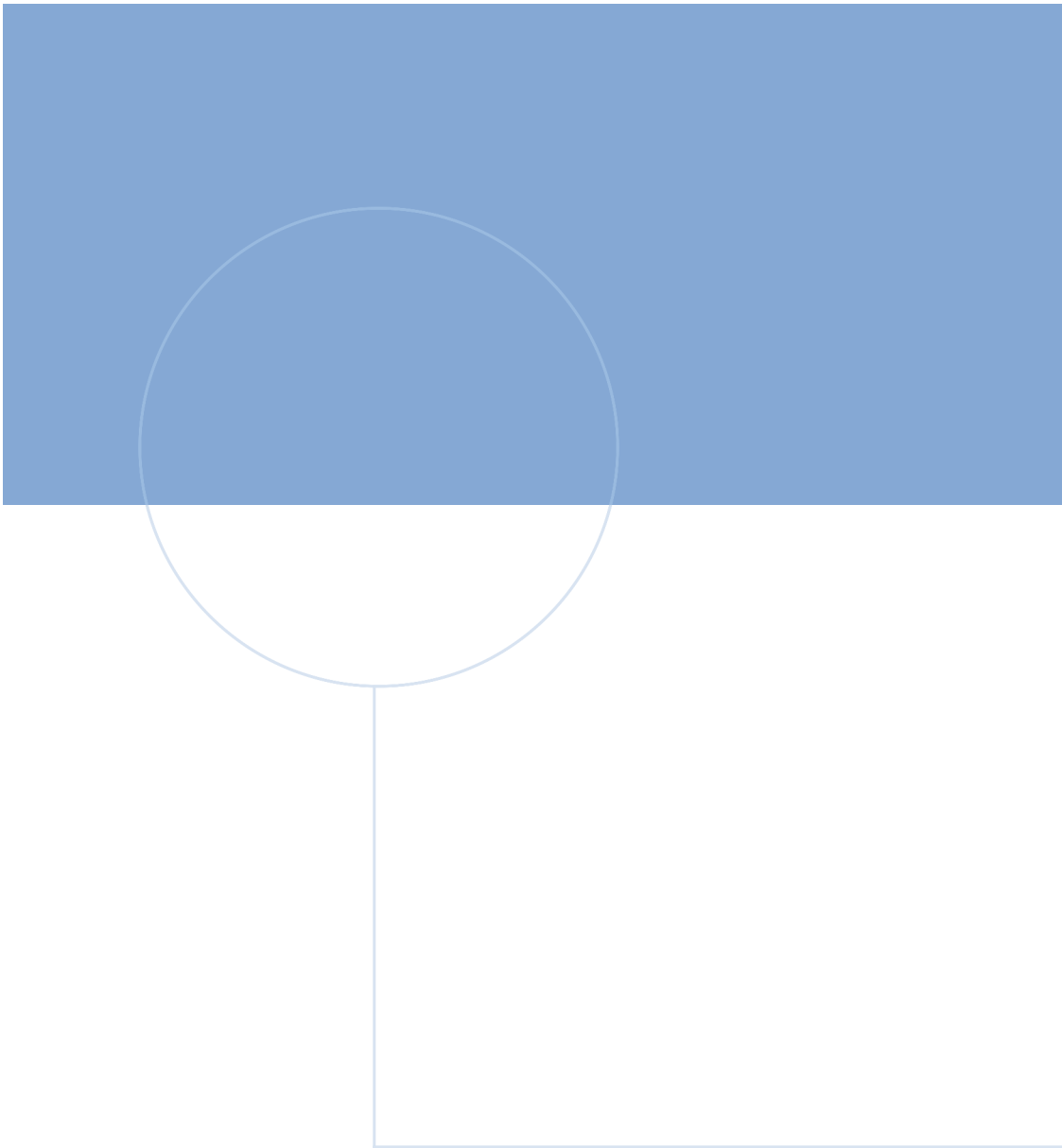

NTNU

Norwegian University of
Science and Technology